RESEARCH ARTICLE

ESPL WILEY

Observations of megacusp dynamics and their coupling with crescentic bars at an open, fetch-limited beach

Rinse L. de Swart[1] | **Francesca Ribas**[1] | **Daniel Calvete**[1] | **Gonzalo Simarro**[2] | **Jorge Guillén**[2]

[1]Department of Physics, Universitat Politècnica de Catalunya (UPC), Barcelona, Spain

[2]Department of Marine Geosciences, Institut de Ciències del Mar (ICM-CSIC), Barcelona, Spain

Correspondence
Rinse L. de Swart, Department of Physics, Universitat Politècnica de Catalunya (UPC), Jordi Girona, 1–3, 08034 Barcelona, Spain.
Email: rinse.de.swart@upc.edu

Abstract

Alongshore changes in shorelines along sandy beaches are a result of variations in wave conditions and nearshore morphology, which can cause straight shorelines to develop large-scale (100–1000 m wavelength) undulations, called megacusps, which cause local shoreline accretion and erosion. Megacusps are often morphologically coupled to alongshore variability in the nearshore sandbar (crescentic bars). Sandbar rhythmicity has been studied extensively, whilst megacusp dynamics and their coupling with crescentic bars have received less attention. This study uses a long-term dataset of hourly time-exposure video images and detailed propagated wave conditions to investigate megacusp dynamics and the corresponding sandbar–shoreline coupling at the low-energetic, tideless beach of Castelldefels (northwestern Mediterranean Sea, Spain). Megacusps were observed during 24% of the study period. Crescentic bars were present during 91% of the days with megacusps, whilst megacusps were not observed during 50% of the days with crescentic bars. Megacusp wavelengths (100–700 m) were comparable to those of crescentic bars, whilst cross-shore amplitudes (3–8 m) and alongshore migration speeds (0–15 m/day) were smaller than those of crescentic bars. No clear relation was observed between wave conditions and megacusp formation, migration and disappearance. However, megacusp presence was strongly linked to crescentic bar presence, as megacusps mostly developed some days after the formation of a crescentic bar. Coupling between shoreline and inner sandbar was significant during 74% of the time with simultaneous presence of megacusps and crescentic bars. No dominance of one particular coupling pattern was observed, although the pattern depended on the wave height and the wave angle. It is hypothesised that the wave height and angle determine the type of flow pattern over the inner crescentic bar (single or double rip cell circulations versus meandering currents) and thus control the type of coupling.

KEYWORDS
beach morphology, Mediterranean Sea, morphological coupling, nearshore patterns, rip cell circulations, rip-channel systems, video monitoring

1 | INTRODUCTION

Shorelines along sandy coasts can display a wide range of morphological patterns due to changes in hydrodynamics and sediment transport.

One example of such patterns are megacusps, which are alongshore shoreline undulations consisting of horns (seaward shoreline protrusions) and embayments (landward shoreline perturbations) that typically have wavelengths of hundreds of metres and cross-shore

amplitudes (half the cross-shore distance between megacusp horns and bays) up to several tens of metres (e.g., Castelle et al., 2015; Segura et al., 2018; Thornton et al., 2007). Similar alongshore variability (consisting of shoreward horns and seaward bays) is often present in nearshore sandbars, in which case they are referred to as crescentic bars or rip-channel systems (e.g., Van Enckevort et al., 2004). Morphological coupling is often present between megacusps and crescentic bars (e.g., Coco et al., 2005; Sonu, 1973; Van de Lageweg et al., 2013) and between inner and outer crescentic bars (e.g., Price & Ruessink, 2013; Ruessink et al., 2007), with the coupling pattern varying significantly between beaches. The coupling between crescentic bars and megacusps is important for coastal management, as the evolution of megacusps can lead to fast changes in shoreline position (Birrien et al., 2013; Thornton et al., 2007). Megacusp formation during low-energetic waves is often linked to overall shoreline accretion (e.g., Segura et al., 2018; Van de Lageweg et al., 2013), whilst megacusp development during storms can induce significant beach and dune erosion at the megacusp embayments (Castelle et al., 2019; Thornton et al., 2007).

Shoreline and sandbar variability has been extensively studied in the past decades. Specifically, the ability to track sandbar variation using video images (Lippmann & Holman, 1989) resulted in a large number of studies investigating crescentic bars (e.g., Price & Ruessink, 2011; Van Enckevort et al., 2004) and, to a lesser extent, megacusps (e.g., Orzech et al., 2011; Segura et al., 2018). Generally, formation of crescentic bars was observed during low-energetic wave conditions with limited obliquity (e.g., Van Enckevort et al., 2004) and bar straightening during more energetic waves or strong oblique angles of incidence (e.g., Contardo & Symonds, 2015). Some previous studies observed megacusps to form during lower energetic conditions and to disappear during storms (e.g., Birrien et al., 2013), although megacusps were also observed to persist during storms (e.g., Aagaard et al., 2005; Quartel, 2009) and to disappear during lower energetic wave conditions (Segura et al., 2018). Large erosive megacusps could also form during storms and cause strong dune erosion (Castelle et al., 2019). Reported megacusp characteristics show a large variety, with average wavelengths ranging from 100 m to 2 km and average cross-shore amplitudes from 3 to 15 m (Castelle et al., 2015; Segura et al., 2018; Thornton et al., 2007). Several studies have also observed alongshore migration of megacusps (e.g., Quartel, 2009; Thornton et al., 2007) with reported rates sometimes exceeding 30 m/day (Galal & Takewaka, 2008).

The coupling between crescentic bars and megacusps has been observed to be in phase and out of phase on timescales up to years (e.g., Castelle et al., 2019; Van de Lageweg et al., 2013) and similar coupling patterns have been observed between inner and outer crescentic bars (e.g., Price & Ruessink, 2013; Ruessink et al., 2007). The coupling patterns between crescentic bars and megacusps in the present study are defined using the position, meaning that in phase coupling corresponds to megacusp embayments in front of shoreward crescentic bar horns and out of phase coupling corresponds to shoreline embayments in front of seaward crescentic bar bays. Note that comparing previous observations of coupling patterns should be done carefully, as earlier studies (e.g., Balouin et al., 2013; Sonu, 1973) often defined coupling patterns based on the bathymetry instead of the position, resulting in exactly opposite definitions of in phase and out of phase coupling.

In recent years, various studies (e.g., Castelle et al., 2010; Price et al., 2013) have demonstrated that there is a clear relation between the wave conditions and the type of coupling between inner and outer crescentic bars. Price and Ruessink (2013) summarised these findings in a conceptual model, which states that the coupling pattern is mainly determined by the wave conditions (wave height and direction) as well as variations in depth along the outer bar. For near shore-normal waves, out of phase (in phase) coupling is linked to the presence of a double (single) rip cell circulation pattern that develops when higher (lower) energetic waves experience breaking (refraction) over the outer bar (Castelle et al., 2010). Furthermore, Price and Ruessink (2013) observed a downdrift shift of the inner bar horn with respect to the outer bar horn, which they attributed to strong oblique wave angles driving a meandering alongshore current over the inner crescentic bar (following MacMahan et al., 2010; Sonu, 1972). This hypothesis was confirmed by a subsequent modelling study (Price et al., 2013) and it is hypothesised that similar mechanisms also play a role in sandbar–shoreline coupling.

Although coupling between crescentic bars and megacusps has been observed regularly in the field and forms an important part of the beach state classification scheme of Wright and Short (1984), nearshore models often use a fixed shoreline (e.g., Garnier et al., 2008). Modelling studies in which the shoreline and sandbar are allowed to evolve generally show out of phase coupling (e.g., Castelle & Ruessink, 2011; Orzech et al., 2011), although these studies mostly do not focus on sandbar–shoreline coupling. To date, there is no consensus regarding the relation between the type of sandbar–shoreline coupling and the wave and tide conditions. Existing model studies show variable results, with some of them (Calvete et al., 2005; Coco et al., 2020) finding a clear relation between coupling patterns and wave energy, whilst Orzech et al. (2011) reported a strong link between coupling patterns and tides. Furthermore, some observational studies (e.g., Orzech et al., 2011; Van de Lageweg et al., 2013) also contradicted each other regarding the relation between coupling patterns and wave energy.

Available observational studies on megacusps and sandbar–shoreline coupling are often limited in time (e.g., Birrien et al., 2013; Quartel, 2009) or temporal resolution (e.g., Sonu, 1973; Thornton et al., 2007). Additionally, they mostly studied beaches with considerable tidal range (> 1 m) and high-energetic (H_{m0} > 1 m) wave conditions (e.g., Castelle et al., 2019; Van de Lageweg et al., 2013) or long fetches (Segura et al., 2018). Only a limited number of studies have focused on low-energetic areas (like the Mediterranean Sea) with insignificant tides and small fetches (e.g., Balouin et al., 2013; Bowman & Goldsmith, 1983) and they mostly used data with limited temporal resolution and/or short study periods. Additionally, they do not provide a detailed analysis of the megacusp dynamics and the coupling between megacusps and crescentic bars. Furthermore, most previous studies on sandbar–shoreline coupling generally only dealt with in phase versus out of phase coupling and overlooked intermediate coupling patterns. As a result, more observations that quantify the various coupling patterns and megacusp formation/disappearance moments are needed for validating model results and to provide further consensus between observations, in particular regarding the relation between coupling patterns and beach conditions.

The objective of the present study is to characterise megacusp events and the coupling between megacusps and crescentic bars, and

to link them to the prevailing wave conditions. This is done for the open, fetch-limited, tideless beach of Castelldefels (northwestern Mediterranean Sea, Spain) using a nearly 8-year dataset of hourly video images and hourly propagated wave conditions. Special attention is given to quantifying the role of directional wave conditions and the bathymetric configuration on megacusp formation/disappearance and the emergence of different coupling patterns (in phase, out of phase and intermediate). After a brief description of the field site and dataset (Section 2), the methods used to collect and characterise the data are described (Section 3). Subsequently, the results of the analysis are presented (Section 4) and contextualised and compared with previous studies (Section 5). Finally, the most important findings are summarised in the conclusions (Section 6).

2 | STUDY AREA AND DATA COLLECTION

2.1 | Study site

Megacusp dynamics and sandbar–shoreline coupling were studied at the open, double-barred beach of Castelldefels, located about 20 km southwest of Barcelona (northwestern Mediterranean Sea; Figure 1). The study site is a 1 km straight beach section with an east–west alignment (89° with respect to north). Castelldefels beach is composed of sand with a median grain size of 270 μm and the average nearshore bed slope is approximately 0.014 (De Swart et al., 2021). Tides are almost absent in this part of the Mediterranean Sea, with a

tidal range of approximately 20 (10) cm during spring (neap) tide, so that it is considered a tideless beach (Simarro et al., 2015). The waves are low-energetic with occasional storms ($H_{m0} > 1.5$ m at deep water Puertos del Estado, 1994) lasting mostly less than 1 day that mainly occur between September and March. The mean significant wave height H_{m0} during the entire study period (October 2010 to August 2018) was 0.73 m at the Barcelona wave buoy (68 m depth), with a mean zero-crossing period T_{m02} of 3.8 s. Wave direction can be separated into two dominant directions (east-southeast and south; De Swart et al., 2020), with average mean wave directions θ_{mean} of 100° and 176° (with respect to north), respectively.

The inner bar or terrace at Castelldefels often becomes crescentic and is generally located between 0 and 50 m from shore, and the outer bar is located 100–200 m from shore (Figure SI-1 in the Supporting Information). Crescentic bar formation at Castelldefels beach strongly depends on the initial bathymetry as it was only observed when the bar–shoreline distance exceeded 10 m (De Swart et al., 2021). Crescentic bars showed a large variability in wavelengths (100–700 m), cross-shore amplitudes (5–20 m) and alongshore migration speeds (0–50 m/day). Wavelengths increased for larger bar–shoreline distances and alongshore migration was strongly related to the radiation stress S_{xy} (the alongshore transport of cross-shore momentum). The sandbar typically became crescentic during lower energetic waves with limited obliquity ($\theta \lesssim 20°$ at 10-m depth), whilst higher energetic waves with strong oblique angles ($\theta \gtrsim 15°$) dominated during bar straightening (De Swart et al., 2021).
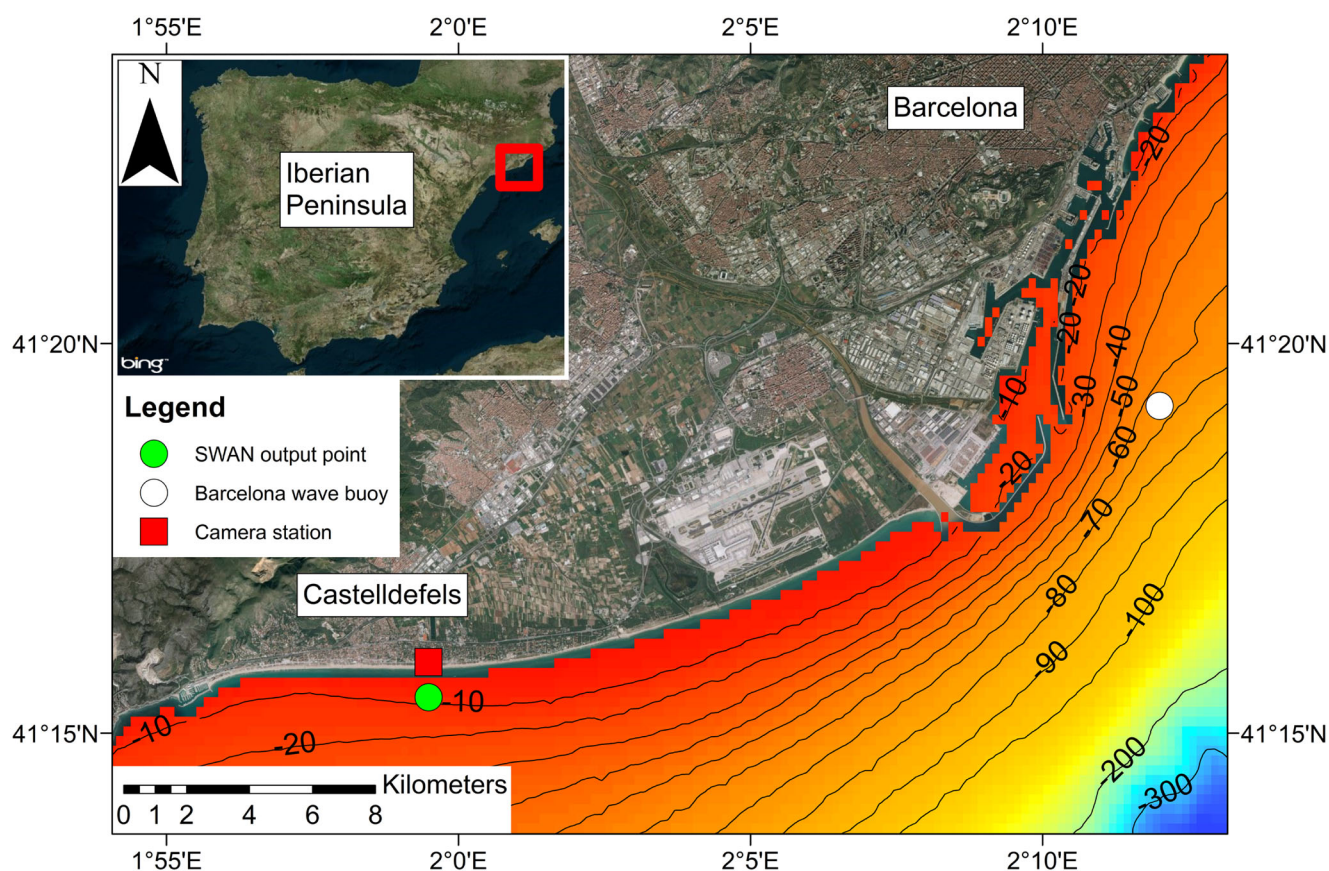

FIGURE 1 Map of the study area showing the study site, the nearshore bathymetry (source Emodnet) and the locations of the Barcelona wave buoy and the SWAN output point. The aerial photography is part of Microsoft Bing Maps (©2022 Microsoft Corporation Earthstar Geographics SIO). Figure from De Swart et al. (2021)

2.2 | Video observations

Video observations have been collected since 5 October 2010 at Castelldefels beach (De Swart et al., 2021). The video monitoring system consists of five cameras that cover a 180° overview of the shoreline and uses the Sirena open source code (Nieto et al., 2010). Each daylight hour, the cameras obtain time-exposure images by averaging 600 snapshots taken during a 10 min period. The Ulises software (Simarro et al., 2017) was used to georeference and rectify the images of the separate cameras and to merge them into a planview spanning 1000 m in the alongshore and 300 m in the cross-shore direction, with a pixel resolution of 0.5 m (Figure SI-2).

In this study, planviews were used that were obtained between 5 October 2010 and 31 August 2018 (2888 days). In case of partial camera failure, planviews were included when at least two adjacent cameras were operational. In total, planviews were available 92% of the time (2664 days), with more than half of the days without images being the result of a renovation of the camera system between October 2016 and January 2017. The same planview dataset was used by De Swart et al. (2021) to track the sandbars during the entire study period by means of detecting the dominant wave-breaking areas in the time-exposure images (from now on called barlines; Figure 2e–h). Barlines could only be tracked for planviews with sufficient wave breaking, but fortunately no visible wave breaking indicates low-energetic wave conditions that will not cause large morphological changes. Normally, one image per day (generally around midday) was used to track the barlines, but up to three images were used on days with rapid changes in the wave-breaking pattern. In total, 2279 barlines were obtained spanning 2208 days.

2.3 | Wave data

Hourly wave conditions were provided by the Barcelona wave buoy (data availability 97% of the time), located in front of Barcelona harbour at 68 m depth (Figure 1). Both the full 2D frequency–direction spectra as well as integrated wave parameters (H_{m0}, T_{m02} and θ_{mean}) were obtained. Subsequently, the buoy data were propagated using
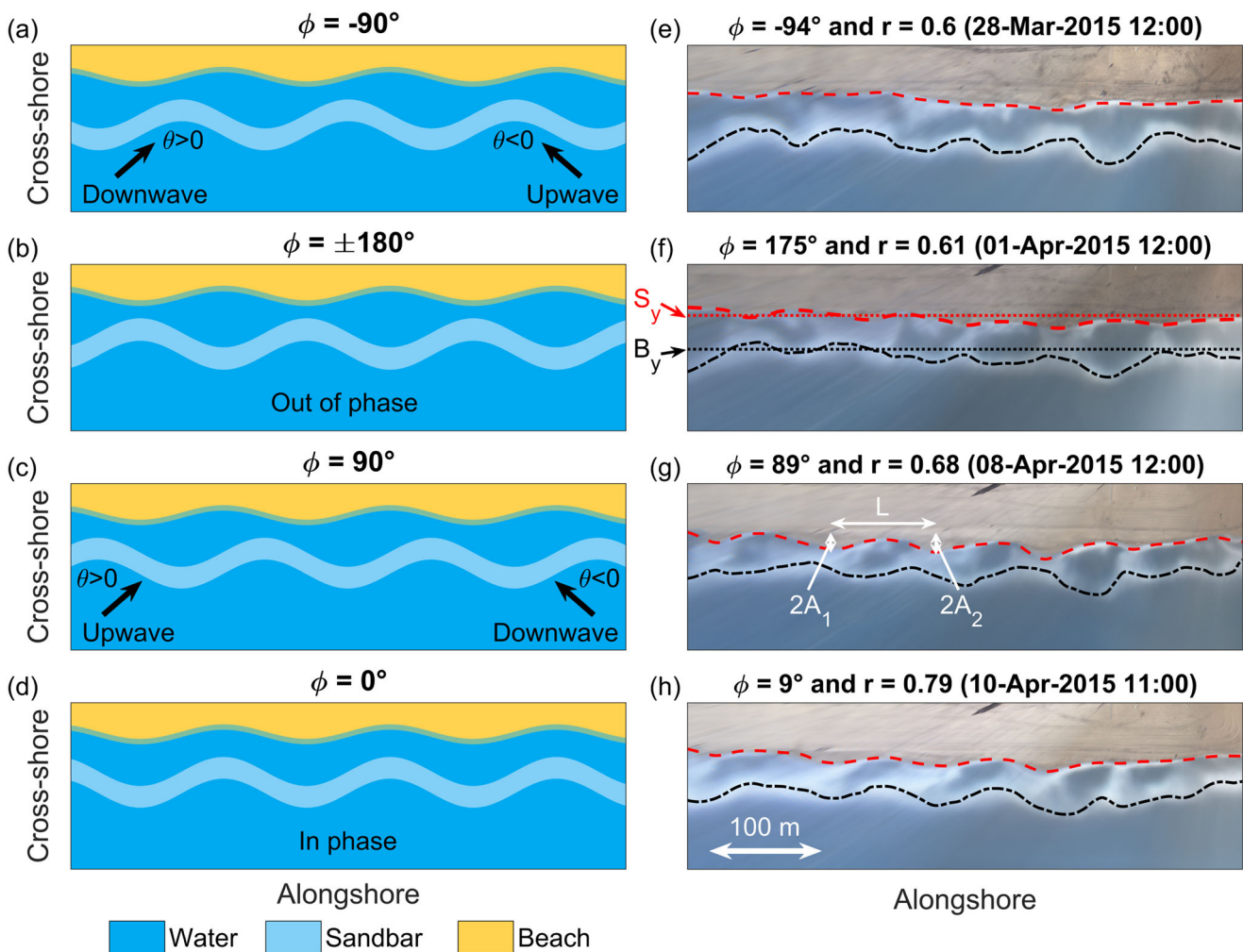

FIGURE 2 Definitions of the different coupling patterns. The left panels show idealised sketches of the four distinguished coupling patterns based on the phase ϕ: (a) $\phi = -90°$ (upwave for easterly waves; downwave for westerly waves); (b) $\phi = \pm180°$ (out of phase; crescentic bar bays located inside the shoreline embayments); (c) $\phi = +90°$ (upwave for westerly waves; downwave for easterly waves); and (d) $\phi = 0°$ (in phase; crescentic bar horns located inside the shoreline embayments). Zoomed planviews (500 m alongshore, 150 m cross-shore) showing examples of the different coupling patterns are shown in panels (e–h) including the computed values for r and ϕ. The tracked bar (black) and shorelines (red) are plotted in all images. Furthermore, panel (f) shows the alongshore-averaged barline and shoreline positions B_y and S_y, whereas panel (g) shows examples of megacusp wavelength L and the double partial amplitudes $2A_1$ and $2A_2$ (the amplitude A is defined as $A = \frac{A_1 + A_2}{2}$)

SWAN (De Swart et al., 2020) to a single output point located at 10-m depth in front of the camera tower. The SWAN model was forced with two types of offshore boundary conditions: measured 2D spectra and measured integrated wave parameters. Only the former one is used in the present analysis because it provides optimal results (best fit with in situ measurements) at the location of interest (particularly regarding θ_{mean}; see De Swart et al., 2020).

Following De Swart et al. (2021), each shoreline and barline was assigned the wave conditions that occurred in the 24 h before midday on the day of the shoreline/barline. In case wave conditions were unavailable during more than 75% of the 24 h or if $H_{m0} < 0.2$ m, the corresponding shorelines and barlines were excluded from the analysis. Wave angles with respect to shore-normal were computed using a constant coastline orientation of 89° with respect to north. Easterly and westerly waves were separated using a boundary of $-5°$ with respect to shore-normal (negative angle indicates east). The reason for this adjustment was the bias in propagated wave direction ($-7.5°$ for easterly and 2.3° for westerly waves; see De Swart et al., 2020). The radiation stress S_{xy} (alongshore transport of cross-shore momentum) was computed using the wave conditions following Holthuijsen (2007).

3 | METHODS

3.1 | Visual analysis and data collection

Megacusp formation and disappearance was visually tracked using daily planview images (at 12:00) by two experienced researchers to reduce subjectivity. The two separate analyses were compared and the disagreements (10% of the time) were cross-checked to obtain the final visual analysis. A megacusp event was defined when three or more shoreline undulations with a clear visually noticeable rhythmicity were present in at least half of the planview domain for a minimum of 2 days. Shorelines with two undulations were also included when the wavelength was such that more undulations did not fit in the planview domain. Megacusp events lasting 1 day were included when a clear rhythmic pattern was present in the entire planview domain. During an image gap, a megacusp event was assumed to continue when the megacusp pattern in the first image after the gap resembled the pattern in the last image before the gap. Specific attention was paid to detecting the moments of megacusp formation and megacusp disappearance. A formation moment was defined as the first day when megacusps were observed in the planview images, following a period without such features. Planview images in which the alongshore variability of the shoreline increased (e.g., a clear increase in megacusp amplitude) were categorised as reinforcement moments and added to the dataset of formation moments. A disappearance moment was defined as the first day in which megacusps were no longer observed following a period with megacusps. Planview images in which the alongshore variability of the shoreline decreased (e.g., a clear reduction in amplitude) but the undulations persisted (same horn/bay locations, identical wavelengths) were categorised as partial disappearance moments and added to the dataset with disappearance moments. All these criteria are consistent with those used by De Swart et al. (2021) for the detection of crescentic bars. The identified megacusp events were further divided into events with and without

crescentic bars by checking whether a crescentic bar was present at some point during each event. Similarly, crescentic bar events were separated into events with and without megacusps.

The uShore software (Ribas et al., 2020) was used to automatically extract the shorelines from all planview images. This methodology uses four standard procedures to detect shorelines and combines these to construct the final accurate shoreline (cross-shore errors below 2.5 m at the study site). The default settings described in Ribas et al. (2020) were used, with the exception of those associated with the space–time filtering of the final shoreline. Here, time filtering was not applied and a 20 m window was used for computing the moving average in space. Subsequently, the shorelines were visually analysed to select the best shoreline per day. For the 145 days without a shoreline of sufficient quality, the shorelines were manually digitised using the best-quality planview image. Finally, all obtained shorelines were subjected to a final visual check to verify that the megacusp undulations were correctly captured. Shorelines that did not meet this requirement were modified to better follow the megacusp undulations in the planview images. In total, one shoreline was obtained for each day with camera images (2664 images in total).

3.2 | Bar and shoreline characterisation

Cross-shore shoreline positions $S(y)$ were obtained for all alongshore positions y (spacing of 0.5 m) of each shoreline. Time series of the alongshore-averaged shoreline positions $S_y(t)$ were computed (Figure 2f), as well as time series of the sinuosity of the shoreline positions $Sin_S(t)$ (Ojeda et al., 2011). An available dataset of barlines (De Swart et al., 2021) was used to obtain the cross-shore barline positions $B(y)$ and the time series of the alongshore-averaged barline positions $B_y(t)$ and the sinuosity of the barline positions $Sin_B(t)$. Finally, time series of the alongshore-averaged sandbar–shoreline distances were obtained ($D_y(t) = B_y(t) - S_y(t)$). The origin of the coordinate system used to describe the shoreline and barline positions is the location of the camera system (41°15′54.7″N, 1°59′29.1″E).

In all shorelines with megacusps, the bays and horns were detected under the conditions that a minimum cross-shore distance of 3 m and a maximum alongshore distance of 500 m existed between a successive bay and horn. These limitations were set to avoid the detection of small (typically short-lived) undulations as megacusps and to make sure that at least one full undulation (two horns and one bay) occurred in the planview domain. For each megacusp (MC) undulation (Figure 2g), the wavelength L_{MC} was computed as the alongshore distance between the horns and the amplitude A_{MC} was computed as half the average cross-shore distance between the bay and the two adjacent horns. Typically, the variation in A_{MC} within the same shoreline was small (average standard deviation of 1 m), whereas the variation in L_{MC} was much larger (average standard deviation of 58 m). Only shorelines in which megacusps were present in at least 40% of the planview domain (combined wavelength of all undulations exceeding 400 m) were used for analysing megacusp characteristics. For each shoreline, the alongshore-averaged wavelengths and amplitudes $L_{y,MC}$ and $A_{y,MC}$ were obtained by averaging L_{MC} and A_{MC}. The alongshore-averaged crescentic bar (CB) wavelengths $L_{y,CB}$ and cross-shore amplitudes $A_{y,CB}$ were obtained analogously (De Swart et al., 2021).

Lastly, alongshore megacusp migration rates were computed by cross-correlating detrended shorelines. Each shoreline that was part of a megacusp event was cross-correlated with shorelines dating between 2 and 4 days after the original shoreline (only if they belonged to the same megacusp event). The alongshore displacement of the megacusps $s_{y,MC}$ is given by the lag belonging to the positive peak located closest to the origin of the cross-correlogram. The direction of migration is indicated by the sign of the lag (positive for eastward migration). A minimum normalized correlation of 0.7 was enforced. To obtain the migration rate $C_{y,MC}$, the displacement $s_{y,MC}$ is divided by the time lag between the two correlated shorelines. Migration speeds of crescentic bars $C_{y,CB}$ were obtained analogously (De Swart et al., 2021).

3.3 | Bar and shoreline coupling

At the study site, only the inner bar was relevant for quantifying the sandbar–shoreline coupling as the outer bar was located too far seaward and was mostly inactive due to insufficient wave energy. Whether the inner sandbar and shoreline were morphologically coupled was evaluated by cross-correlating the detrended barline $\hat{B}(y)$ with the detrended shoreline $\hat{S}(y)$ of the same day (e.g., Price & Ruessink, 2013; Rutten et al., 2018). The cross-correlation ρ between $\hat{B}(y)$ and $\hat{S}(y)$ was computed as

$$\rho(\Delta y) = \frac{R_{\hat{B}\hat{S}}(\Delta y)}{\sqrt{R_{\hat{B}\hat{B}}(0)R_{\hat{S}\hat{S}}(0)}}, \quad (1)$$

where $R_{\hat{B}\hat{S}}(\Delta y)$ is the covariance function of $\hat{B}(y)$ shifted over a spatial lag Δy ($\hat{B}(y+\Delta y)$) and $\hat{S}(y)$ at time t along the whole domain (Ruessink et al., 2007). The lag Δy corresponding to the largest $|\rho|$ value indicates the alongshore displacement of the inner sandbar undulations with respect to those in the shoreline, where positive (negative) lags indicate eastward (westward) displacements. The ρ value can vary between -1 (maximum negative correlation) and $+1$ (maximum positive correlation). The 98% confidence interval of significant cross-correlation was computed using a reduced number of effective points (Garrett & Toulany, 1981), following Price and Ruessink (2013).

In previous studies (e.g., Rutten et al., 2018), $\rho < 0$ was assumed to correspond to out of phase coupling (crescentic bar bays located inside the shoreline embayments; Figure 2b) and $\rho > 0$ to in phase coupling (crescentic bar horns located inside the shoreline embayments; Figure 2d). However, this only applies when $|\Delta y|$ belonging to the largest $|\rho|$ value does not exceed a quarter of the wavelength of the coupled pattern. This was not always true in the current dataset (see example in Figure SI-3), which meant that additional analysis was required to identify the coupling types and to characterise the phase between the two signals. First, the lag corresponding to the largest $|\rho|$, called Δy_{max}, was detected in the interval $\left[-\frac{1}{2}L_{y,CB} \leq \Delta y \leq \frac{1}{2}L_{y,CB}\right]$, where $L_{y,CB}$ are the crescentic bar wavelengths. The corresponding absolute largest correlation value, called r, was also obtained ($r = |\rho(\Delta y_{max})|$). When $|\Delta y_{max}| > \frac{1}{4}L_{y,CB}$, the coupling type is opposite to that suggested by the sign of $\rho(\Delta y_{max})$. This was taken into account by computing the phase ϕ (wrapped to the interval $[-180°, +180°]$) following

$$\phi = 360° \frac{\Delta y_{max}}{L_{y,CB}} \text{ when } \rho(\Delta y_{max}) \geq 0, \quad (2)$$

$$\phi = 360° \frac{\Delta y_{max}}{L_{y,CB}} - 180° \text{ when } \rho(\Delta y_{max}) < 0. \quad (3)$$

Using this methodology, $\phi = 0°$ always corresponds to in phase coupling (Figure 2d) and $\phi = \pm 180°$ always corresponds to out of phase coupling (Figure 2b). Taking out of phase coupling as reference, the intermediate cases of $\phi = -90°$ and $\phi = +90°$ were classified as upwave or downwave (depending on the angle of incidence θ; Figure 2a,c). Downwave (upwave) coupling indicates that the crescentic bar horn has migrated downdrift (updrift) with respect to the megacusp horn in the out of phase reference case. The lags were non-dimensionalised using the crescentic bar wavelengths because, compared to megacusps, crescentic bars were generally more pronounced in the planviews.

Since barlines and shorelines were normalised during cross-correlation, numerous cases of significant sandbar–shoreline coupling were obtained during periods with a straight barline and shoreline. Therefore, this article only analyses sandbar–shoreline coupling during days on which both a crescentic bar and megacusps were present at the study site.

4 | RESULTS

4.1 | Shoreline dynamics and megacusp presence

During the study period, the alongshore-averaged shoreline position S_y (with respect to the camera tower) varied between 130 and 170 m, although S_y was mostly close to 150 m (Figure 3d) and typically only showed limited short-term variation. A long-term erosional trend in S_y of approximately 8 m was observed during the study period. In contrast to S_y, the alongshore-averaged sandbar positions B_y showed a lot of variability. Six sandbars were tracked during the study period (always two simultaneously), which displayed fast offshore migration (up to 70 m/day) during significant storms and gradual onshore migration during calmer conditions (Figure 3a,d). Fast offshore migration of the inner sandbar sometimes resulted in the formation of a new sandbar at the shoreline (De Swart et al., 2021). Furthermore, the alongshore variability of the sandbars B was generally much larger compared to that of the shorelines S (compare the sinuosity values in Figure 3e,g).

A total of 67 megacusp events were detected during the study period spanning 706 days (Table 1), meaning that megacusps were present during 24% of the time. No clear seasonal signal exists in the occurrence of megacusps, but they occurred unequally over the study period (Figure 3f). Megacusps were frequently observed during 2013–2017, whilst in 2011–2012 and 2018 there were long periods in which they were not present. Megacusp events also varied significantly in duration during the study period (from days to months). These longer-lasting events are often related to extended periods with low-energetic wave conditions. This leads to the sandbar and shoreline morphology being mostly frozen (arrested; Ojeda et al., 2011) and only diffusion can cause small morphological changes until the wave energy increases.
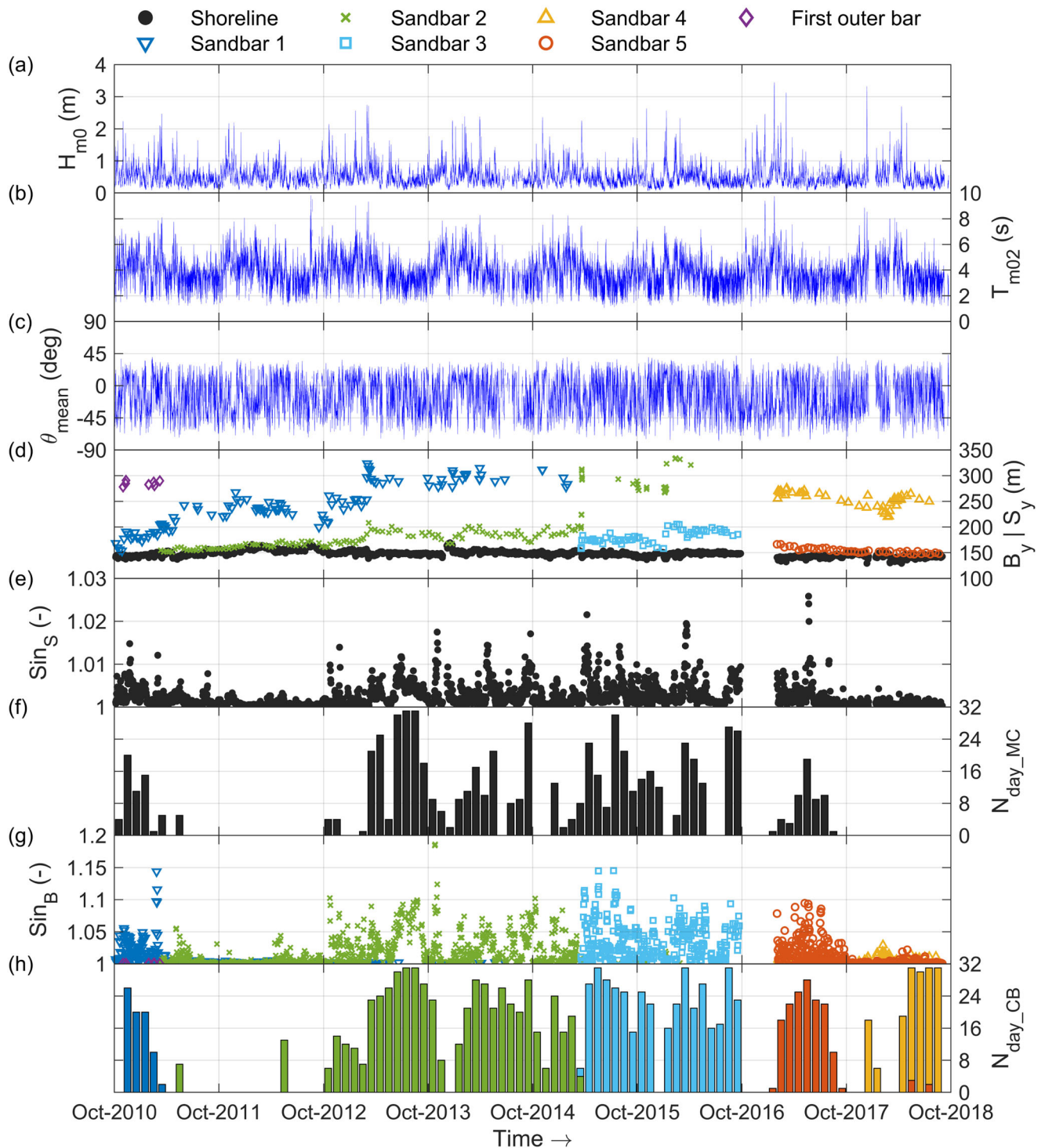
FIGURE 3 (a) Significant wave height H_{m0}, (b) mean period T_{m02}, (c) mean wave direction θ_{mean} from shore-normal (positive for westerly waves), (d) alongshore-averaged bar crest and shoreline positions B_y and S_y (with respect to the camera tower), (e) sinuosity of the shoreline Sin_S, (f) number of days per month with megacusps $N_{day,MC}$, (g) sinuosity of the barlines Sin_B and (h) number of days per month with crescentic bars $N_{day,CB}$ versus time at Castelldefels beach. Panels (a), (b) and (c) display all hourly wave conditions at 10-m depth in front of the study site (no threshold in H_{m0}). To increase readability, only a selection of data points of sandbars 1–5 are shown in panel (d). In case crescentic bars occurred in two different sandbars during the same month (e.g., May and July 2018), the bar with the least number of days with crescentic bars is shown at the front in panel (h)

Generally, megacusps were present together with crescentic bars (Figure 3f,h). There were only five megacusp events (lasting in total 22 days) during which no crescentic bars occurred (Table 1) and crescentic bars were only absent during 9% of all days with megacusps. Note that during megacusp events without crescentic bars an inner bar or terrace is typically present in only half of the

planview (in the other half the waves break directly at the shore-line), which explains the small value for the bar–shoreline distance D_y. Conversely, crescentic bars could occur more frequently without the presence of megacusps (Figure 3f,h) and megacusps were not present during 50% of the days with crescentic bars. In total, 41 crescentic bar events (lasting 218 days) were observed during which no

TABLE 1 Statistics of all megacusp (MC) and crescentic bar (CB) events (inner bar only) during the entire study period and the corresponding mean bar and shoreline characteristics (mean absolute values for C_y)

Event type	Number of events	Mean duration (days)	Total duration (days)	S_y (m)	B_y (m)	D_y (m)	L_y (m)	A_y (m)	C_y (m/day)
CB events with MC	55	18	1005	—	180	33	195	9	4.7
CB events without MC	41	5	218	—	178	29	201	6	3.8
MC events with CB	62	11	684	147	—	32	230	4	1.1
MC events without CB	5	4	22	151	—	8	238	4	1.8

Note: Crescentic bar events are separated in events with megacusp presence and events without megacusp presence. Megacusp events are separated in events with crescentic bar presence and events without crescentic bar presence.
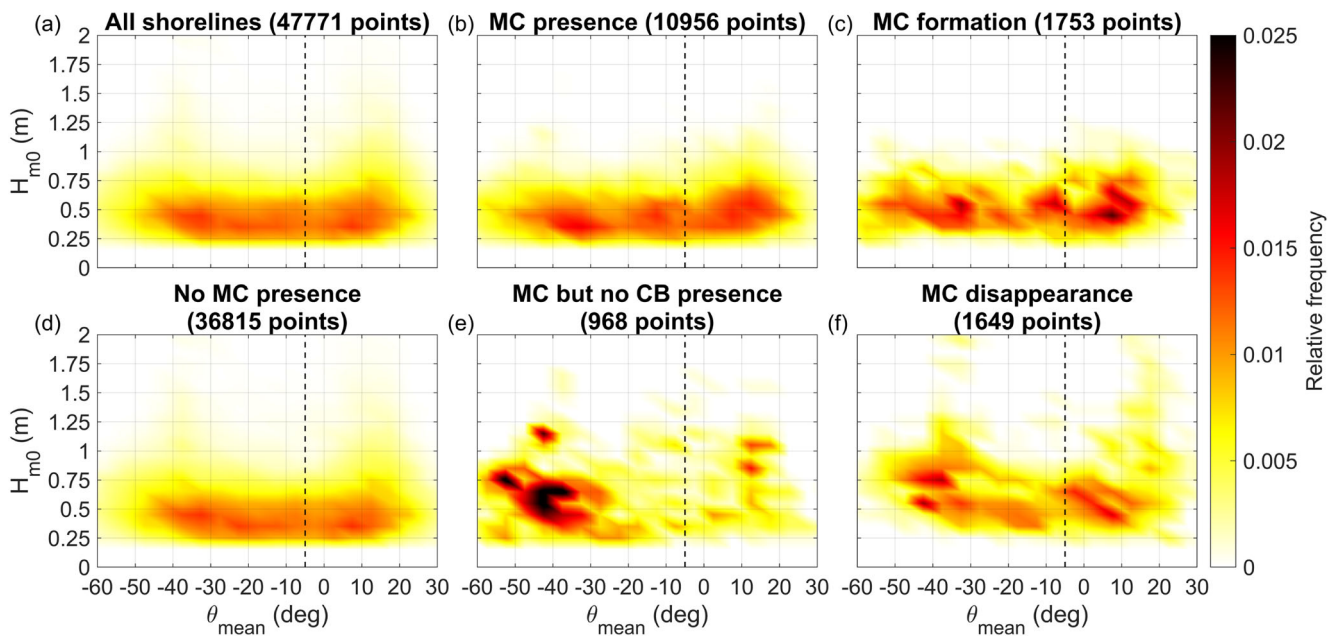

FIGURE 4 2D histograms of hourly significant wave height H_{m0} versus hourly mean wave direction θ_{mean} from shore-normal (positive for westerly waves) at 10-m depth for different categories (MC denotes megacusp and CB denotes crescentic bar). Only data from the SWAN simulation forced with 2D spectra is shown and waves with H_{m0} < 0.2 m are excluded. The dashed vertical line is the separation between easterly and westerly waves
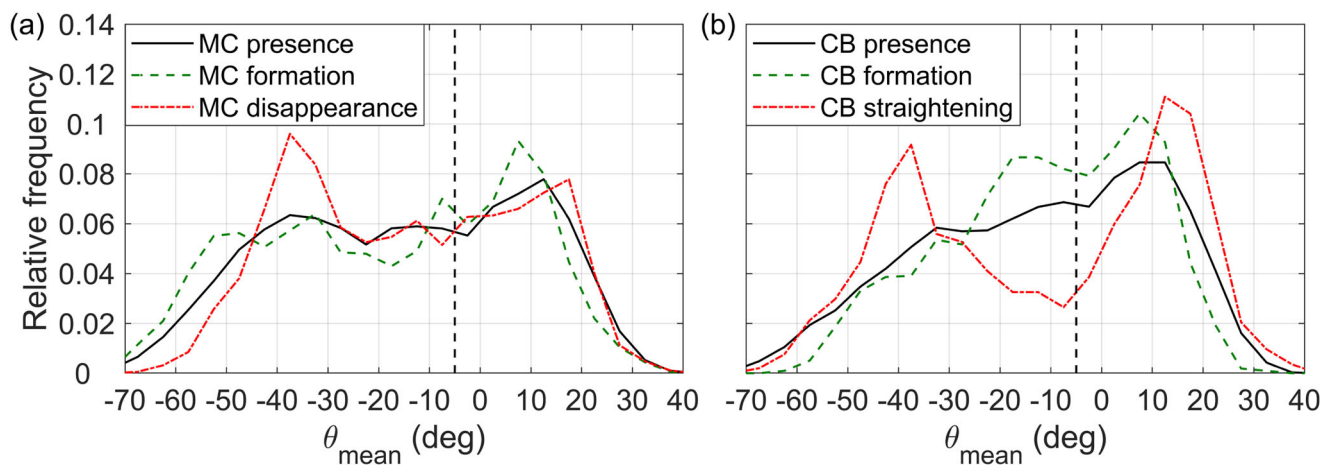

FIGURE 5 Distributions of θ_{mean} at 10-m depth during (a) megacusp presence, formation and disappearance and (b) crescentic bar presence, formation and straightening (taken from De Swart et al., 2021). The dashed vertical line is the separation between easterly and westerly waves
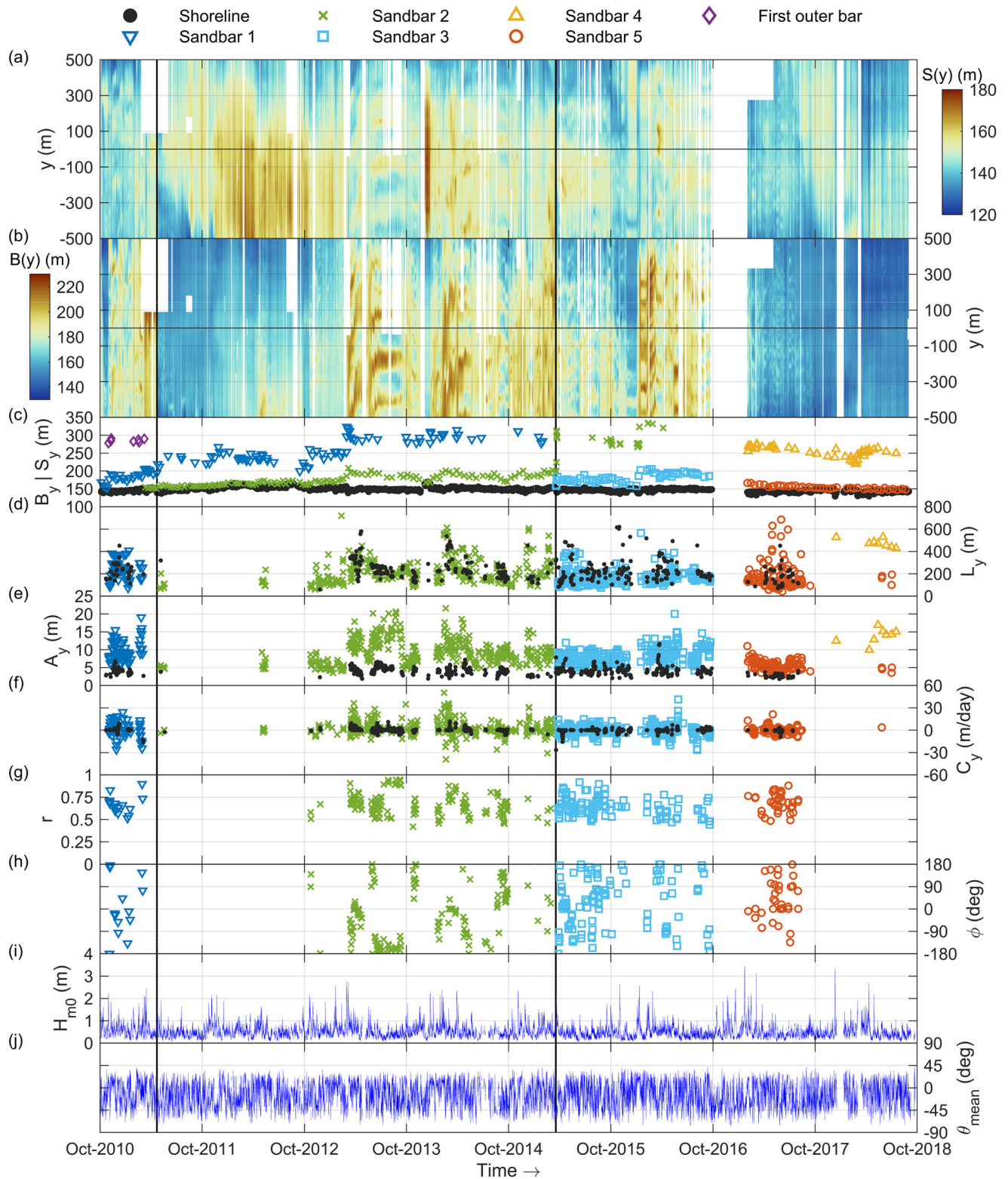
FIGURE 6 The (a) cross-shore shoreline positions (with respect to the camera tower) S at alongshore position y (timestack), (b) cross-shore bar crest positions (with respect to the camera tower) B at alongshore position y of the bar closest to shore (timestack), (c) alongshore-averaged bar crest and shoreline positions B_y and S_y (with respect to the camera tower), (d) alongshore-averaged wavelength L_y, (e) alongshore-averaged amplitude A_y, (f) average migration speed C_y (positive for eastward migration), (g) max correlation r for all moments with significant correlation (98% confidence level) between crescentic bars (inner bar) and megacusps, (h) phase ϕ between crescentic bars (inner bar) and megacusps corresponding to r, (i) significant wave height H_{m0} and (j) mean wave direction θ_{mean} from shore-normal (positive for westerly waves) versus time at Castelldefels beach. The black vertical lines indicate the separation between different sandbars in panel (b). To increase readability, only a selection of data points of sandbars 1–5 are shown in panel (e). Panels (i) and (j) display all hourly wave conditions (at 10-m depth without threshold in H_{m0})

megacusps occurred (Table 1). This indicates that megacusp occurrence strongly depends on crescentic bar presence, whilst the reverse is not true.

4.2 | Megacusp formation/disappearance

The long study period allowed for a detailed study of the conditions leading to megacusp events, including instances of megacusp formation and disappearance. The following analysis focuses on the role of the prevailing wave conditions and the effect of the bathymetric configuration on megacusp formation and disappearance. Histograms of

the wave height and wave direction are shown in Figure 4 for six categories: all days with shorelines (a), days with megacusp presence (b), megacusp formation moments (c), days without megacusps (d), days with megacusps but without crescentic bars (e) and megacusp disappearance moments (f). A comparison of the wave direction distribution during presence, formation and disappearance of megacusps and crescentic bars is shown in Figure 5. Time series showing an overview of all megacusp and crescentic bar data during the entire study period are shown in Figure 6, whilst a representative nearly 2-month period with both megacusp events and crescentic bar events is shown in Figure 7. A selection of planviews corresponding to this period is shown in Figures 2e–h and SI-2.
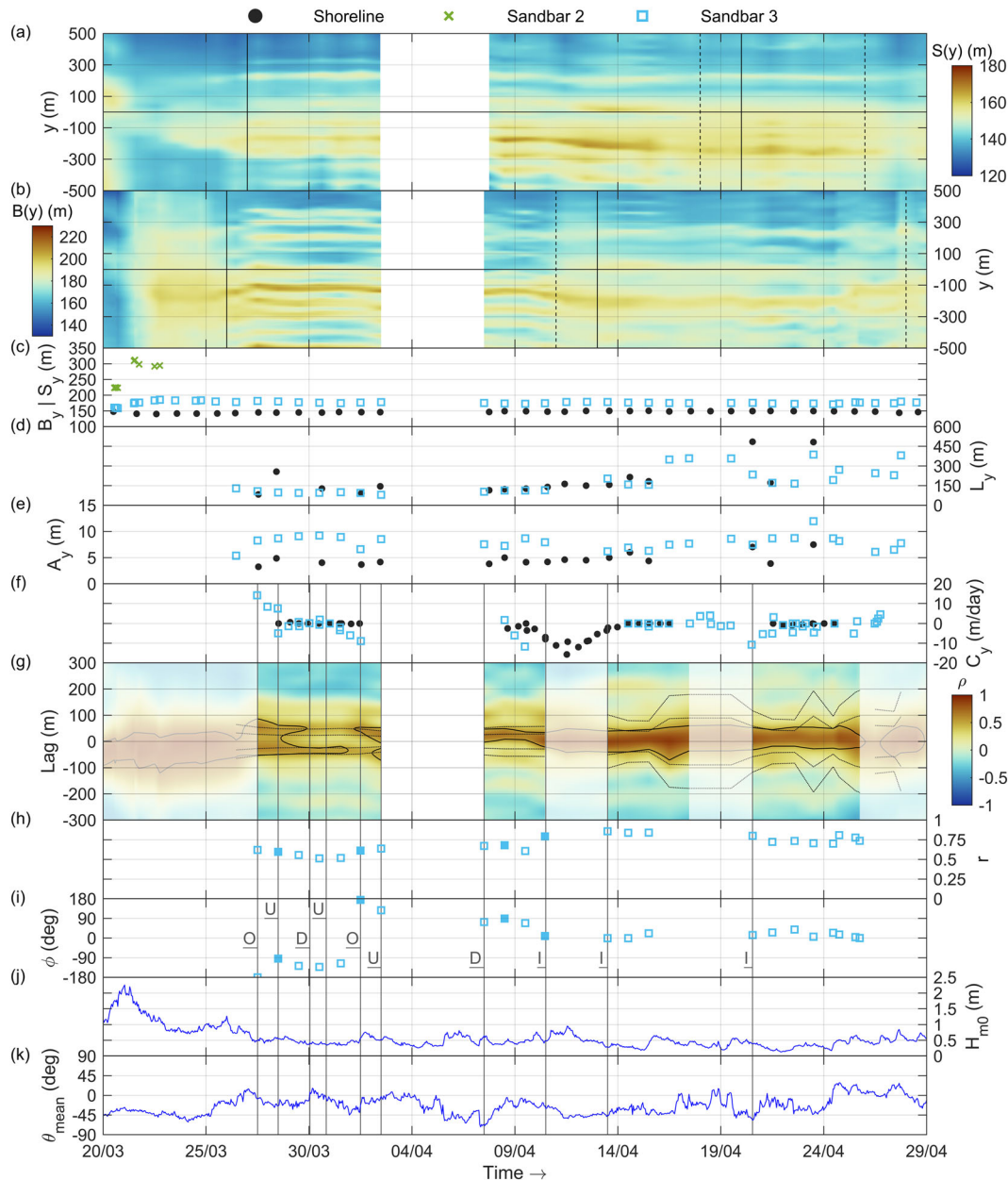

FIGURE 7   Nearly identical to Figure 6, but now showing a zoom-in of a period with sandbar–shoreline coupling in March–April 2015. Panels (a)–(f) are similar to Figure 6, whereas panels (h)–(k) correspond to panels (g)–(j) in Figure 6. Panel (g) shows a timestack of cross-correlation ρ between the inner sandbar and shoreline for different lags (transparent parts indicate periods without crescentic bars and/or megacusps). The black contours in panel (g) indicate the 98% confidence level for statistically significant coupling and the dashed lines indicate $\pm\frac{1}{4}L_{y,CB}$ and $\pm\frac{1}{2}L_{y,CB}$ ($L_{y,CB}$ being the crescentic bar wavelengths). The solid (dashed) vertical lines in panels (a) and (b) indicate the start (end) of a megacusp/crescentic bar event. Furthermore, the grey vertical lines in panels (f)–(k) denote changes in the observed coupling pattern, with the letters in panel (i) denoting the coupling type (O for out of phase coupling, U for upwave coupling, D for downwave coupling and I for in phase coupling). Finally, the filled squares in panels (h) and (i) correspond to the days of the planviews shown in Figure 2

Figure 4a highlights that the entire study period was characterised by mostly calm wave conditions with a large variety in wave angles. The range in wave angles is similar for all categories in Figure 4, whilst some differences in wave height exist between the different categories. Similar wave conditions prevailed when no megacusps were present (Figure 4d), but also during megacusp presence (Figure 4b) and during megacusp formation (Figure 4c). The main difference is that high-energetic waves were completely absent during megacusp presence and megacusp formation. In fact, megacusps typically developed at the study site during periods with relatively low-energetic wave conditions and a large range of incidence angles following a short period with higher energetic wave conditions (e.g., Figure 7 on 21 and 27 March 2015). Higher energetic waves were present during megacusp disappearance (Figure 4f), although the wave angles were less oblique compared to megacusp formation. Furthermore, both low- and high-energetic waves with strong oblique angles (showing a clear dominance of easterly waves) were observed when megacusps were present but crescentic bars were absent (Figure 4e), although this only occurred sporadically. Generally, no clear relation between megacusp formation, migration and disappearance and the wave conditions can be deduced from Figure 4. An analysis of the wave climate and directional spreading also showed limited differences between most of the categories (Figures SI-4 and SI-5). The only notable deviations are a clear dominance of easterly waves during the scarce megacusp events without crescentic bar presence and slightly lower directional spreading values for the same category and during megacusp disappearance. Conversely, crescentic bar dynamics depended strongly on the wave conditions, such as the wave height and especially the wave angle (De Swart et al., 2021). A clear dominance of shore-normal waves was observed during crescentic bar formation, whilst oblique waves were dominant during crescentic bar straightening (Figure 5b). In contrast, the wave angles during megacusp formation and disappearance were not that different (Figure 5a).

The analysis in Section 4.1 already indicates that crescentic bar presence played a major role in megacusp formation. This is further supported by Table 2, which describes the number of days between megacusp and crescentic bar formation (positive numbers indicate a crescentic bar existed before a megacusp formed), and similarly for disappearance and presence. As shown in the first row of Table 2, megacusps mostly formed some days after the formation of a crescentic bar (e.g., Figure 7a,b on 26 and 27 March 2015), although megacusps sometimes developed halfway through a long-lasting

crescentic bar event (e.g., Figure 7a,b on 19 April 2015). Generally, megacusps persisted during calm wave conditions as long as the crescentic bars remained (bottom row of Table 2). Megacusp disappearance often occurred simultaneously with crescentic bar straightening (particularly during high-energetic storms), although megacusps often also disappeared a few days before or after straightening of a crescentic bar during lower energetic wave conditions (middle row of Table 2). Very low-energetic wave conditions led to bar arrestment (no morphological changes in the sandbars), during which only diffusion caused some small-scale morphological changes at the shoreline. One such period occurred in summer 2013 (Figure 6a,b).

4.3 | Megacusp shape and migration

Throughout the study period, megacusp characteristics were very variable (Figure 6d–f) and could also fluctuate substantially within the same event (Figure 7d–f). Megacusp wavelengths were generally quite similar to the crescentic bar wavelengths (Figure 6d and Table 1), although substantial deviations could sometimes occur. In the first days of megacusp events, the wavelengths often deviated from the crescentic bar wavelengths (Figure 7d on 28 March 2015 and 20 and 23 April 2015). Observed megacusps wavelengths can sometimes be larger than those of the crescentic bars because megacusps are generally much more subtle and thus more difficult to detect (especially at the start and end of megacusp events). As a result, megacusp wavelengths were sometimes even unavailable during megacusp events (e.g., Figure 7d on 29 March and 16 and 22 April 2015). In longer-lasting (more than 1 week) events, the wavelengths typically became more similar to the crescentic bar wavelengths as additional megacusps developed (Figure 7d between 7 and 15 April 2015). At the end of megacusp events, the megacusp wavelengths often increased as smaller megacusps disappeared more easily than larger megacusps. All this variability explains the scatter in Figure 8, although the relation is highly significant at the 99% confidence level.

The cross-shore amplitudes of the megacusps were much less variable (Figure 6e). At the start of megacusp events, the amplitudes were generally small (below 5 m; Figure 7e on 27 March 2015) and they slightly increased during longer-lasting events (compare the amplitudes on 30 March and 14 February 2015; Figure 7e). Megacusp amplitudes hardly exceeded 7 m, being much smaller than the amplitudes of crescentic bars (10–20 m; Figure 6e and Table 1).

TABLE 2 Overview for all megacusp events of the differences between (1) the day of megacusp (MC) formation and the closest day of crescentic bar (CB) formation; (2) the day of megacusp disappearance and the closest day of crescentic bar disappearance; and (3) the days with megacusp presence and the closest day of crescentic bar presence

| Category | Number of days difference | | | | | | |
| | MC prior to CB | | | | CB prior to MC | | |
	≤ − 3	−2	−1	0	1	2	≥ 3
Formation	5	0	2.5	5	12.5	11.3	63.7
Disappearance	18.3	4.9	8.5	32.9	15.9	7.3	12.2
Presence	1.5	0.3	0.5	91.2	2.1	1.5	2.9

Note: Results were grouped into bins according to the number of days difference (positive value indicates CB preceded MC) that were subsequently converted to percentages.

The alongshore migration rates of the megacusps were small compared to the crescentic bar migration rates (Figure 6f and Table 1). Megacusps generally migrated with a certain time lag in response to crescentic bar migration (Figure 7f between 9 and 14 April 2015), with migration rates of mostly only a few metres per day that rarely reached more than 10 m/day. No clear relation exists between the megacusp migration rates and the radiation stress S_{xy} (Figure 9). Often, no migration was observed for large S_{xy} values, resulting in small correlation coefficients. This trend is

independent of the time period that was used to compute the migration rates (see Section 3.2).

4.4 | Crescentic bars and megacusps coupling

Two findings that indicate that the inner crescentic bar and the observed megacusps were morphologically coupled are the observed link between megacusp development and crescentic bar presence
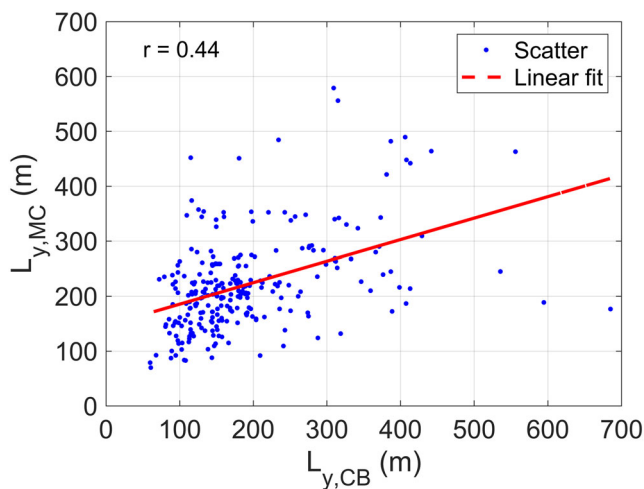

FIGURE 8 Megacusp wavelengths $L_{y,MC}$ plotted versus the crescentic bar wavelengths $L_{y,CB}$ including linear fit and Pearson correlation coefficient. Only moments with significant sandbar–shoreline coupling (98% confidence interval) are shown
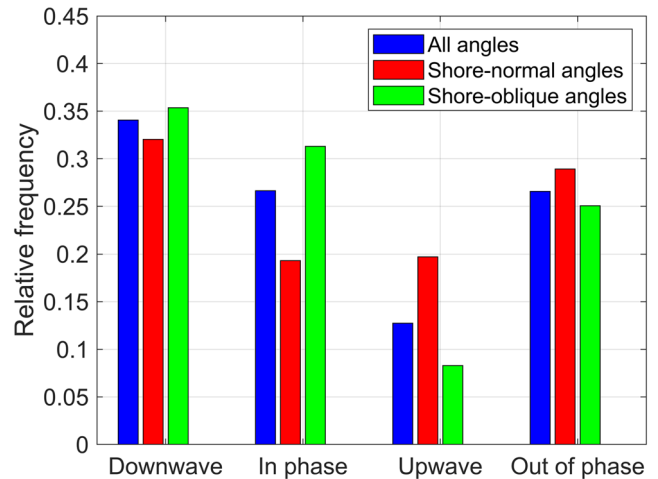

FIGURE 10 Distribution of the different coupling patterns (see Figure 2 and Section 3.3) during the entire study period for different intervals in mean wave direction θ_{mean}: all angles, shore-normal angles ($-20° \leq \theta_{mean} \leq +10°$) and oblique angles ($\theta_{mean} < -20°$ & $\theta_{mean} > +10°$)
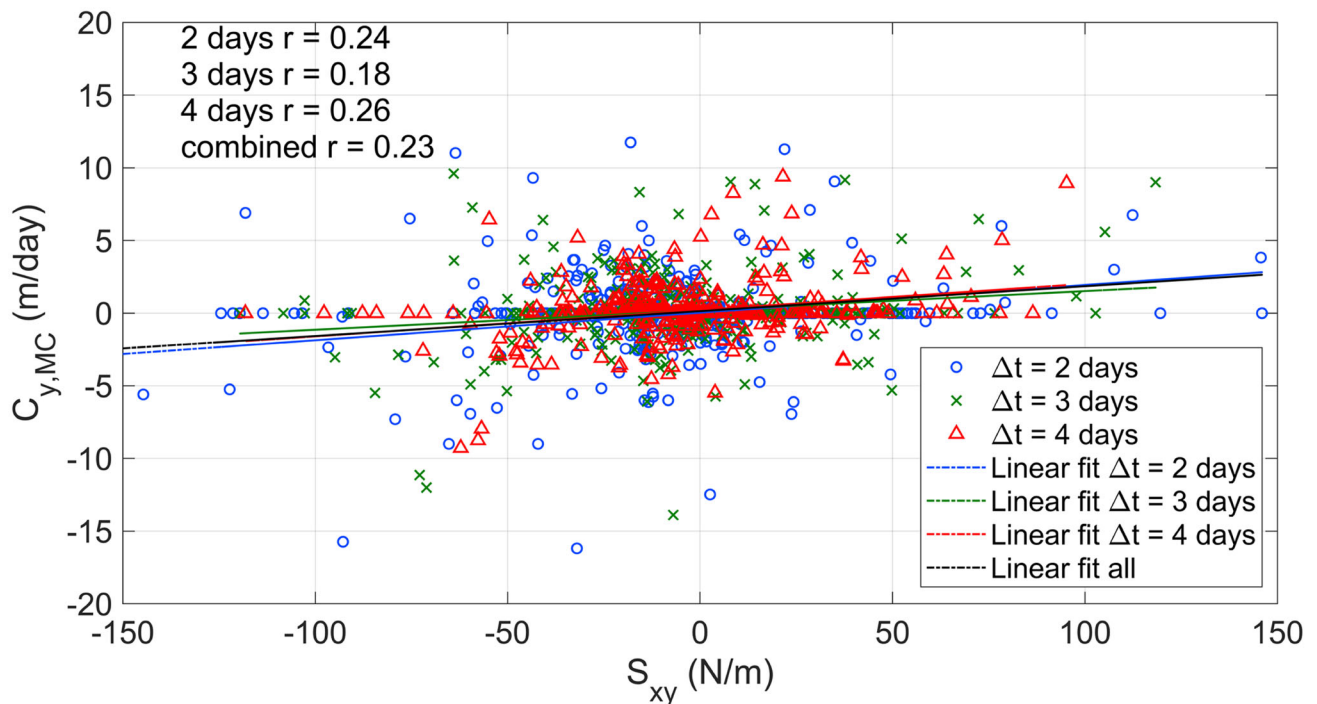

FIGURE 9 Average megacusp migration rate $C_{y,MC}$ (positive for eastward migration) versus radiation stress S_{xy} (positive for waves coming from the west). Linear fits and the corresponding Pearson correlation coefficients are also included. The different colours indicate the time period over which the migration speed was computed. For each migration speed, S_{xy} was averaged over the corresponding time period. When computing S_{xy}, the bias in wave direction was compensated by adding 5° to the wave angles (see Section 3)

(Section 4.2), along with the relation between megacusp and crescentic bar wavelengths (Section 4.3). More evidence was obtained by computing the cross-correlation coefficient ρ (Section 3.3). Throughout the days with simultaneous presence of megacusps and crescentic bars (22% of the study period), the coupling was significant at the 98% confidence level during 74% of the time. Altering the confidence level to 95% or 90% did not cause notable changes to the results.

At Castelldefels, a broad range of coupling patterns was observed during the days with significant coupling (blue bars in Figure 10). The coupling type also partially depended on the wave height and angle. Taking into account all wave directions (blue bars in Figure 10), downwave coupling was most prominent (34% of the time), followed closely by in phase and out of phase coupling (both 27% of the time), whilst upwave coupling was observed less frequently (13% of the time). A similar distribution in coupling patterns was observed for oblique waves (green bars in Figure 10). Conversely, upwave coupling occurred as frequently as in phase coupling during shore-normal waves (20% of the time; red bars in Figure 10), although downwave and out of phase coupling (both about 29% of the time) were still the most common. In phase coupling was mostly observed for higher energetic waves, whilst out of phase coupling occurred mostly during lower energetic waves (Table 3 and Figure SI-8). Intermediate wave conditions were dominant during upwave and downwave coupling. No clear relation was observed between the different coupling patterns and the bar–shoreline distance (Table 3 and Figure SI-9).

An example of a cross-correlogram showing clear sandbar–shoreline coupling is given in Figure 7g for the period March–April 2015 (the cross-correlograms of the entire study period are shown in Figures SI-6 and SI-7). Coupling periods during the study period were often characterised by substantial changes in phase ϕ (Figures 7i, SI-6 and SI-7). Changes in phase were linked to a displacement of the crescentic bar with respect to the megacusps (Figure 11). This is clear for the time period shown in Figure 7. Particularly during the first and second coupling period (27 March–2 April 2015 and 7–10 April 2015), migration of the crescentic bar caused several changes in the coupling pattern (Figure 7f,i). The last two coupling periods showed very little migration of the crescentic bars and megacusps (probably due to the prevailing low-energetic wave conditions; Figure 7f,j on 13–17 and 20–25 April 2015), which resulted in continuous in phase coupling during both periods (Figure 7i).

5 | DISCUSSION

5.1 | Accuracy of megacusp detection

As explained in Section 3.1, megacusp events in this study were detected visually (analogous to crescentic bar events in De Swart et al., 2021) by two experienced researchers to avoid prejudice and increase accuracy. However, previous studies often used the standard deviation (σ; e.g., Rutten et al., 2018) or sinuosity (Sin; Ojeda et al., 2011) to detect alongshore variability in the barline or shoreline. In order to check whether these parameters could be used in the present study for the detection of megacusps, the standard deviations and sinuosities of the shoreline (σ_S and Sin_S, respectively) were obtained for all days with and without visually detected megacusps (Figure 12). Comparing the two parameters shows that Sin_S is a better proxy for megacusp presence compared to σ_S, but there is a range in Sin_S (1.002–1.003) where this parameter is indecisive. To obtain maximum accuracy, it was decided to use the visual analysis in the present study.

Compared to crescentic bars, shoreline undulations were generally less pronounced (particularly in cross-shore amplitude). Megacusp
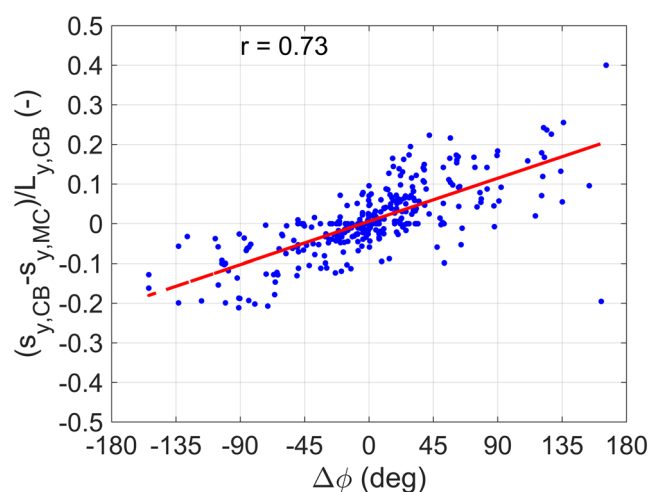

FIGURE 11 Scatter plot of difference between crescentic bar and megacusp displacements (normalised using crescentic bar wavelengths $L_{y,CB}$) versus difference in phase ϕ. Linear fit and the corresponding Pearson correlation coefficient are also included

TABLE 3 Mean values of significant wave height H_{m0} and alongshore-averaged bar–shoreline distance D_y for the four distinguished coupling patterns

Parameter	θ_{mean} category	Coupling patterns			
		Downwave	In phase	Upwave	Out of phase
H_{m0}	All angles	0.49	0.57	0.52	0.47
	Shore-normal angles	0.54	0.58	0.54	0.48
	Shore-oblique angles	0.48	0.57	0.53	0.47
D_y	All angles	31	33	32	34
	Shore-normal angles	36	38	35	34
	Shore-oblique angles	30	32	33	35

Note: Values are given for three different intervals in mean wave direction θ_{mean}: all angles, shore-normal angles ($-20° \leq \theta_{mean} \leq +10°$) and oblique angles ($\theta_{mean} < -20°$ & $\theta_{mean} > +10°$).
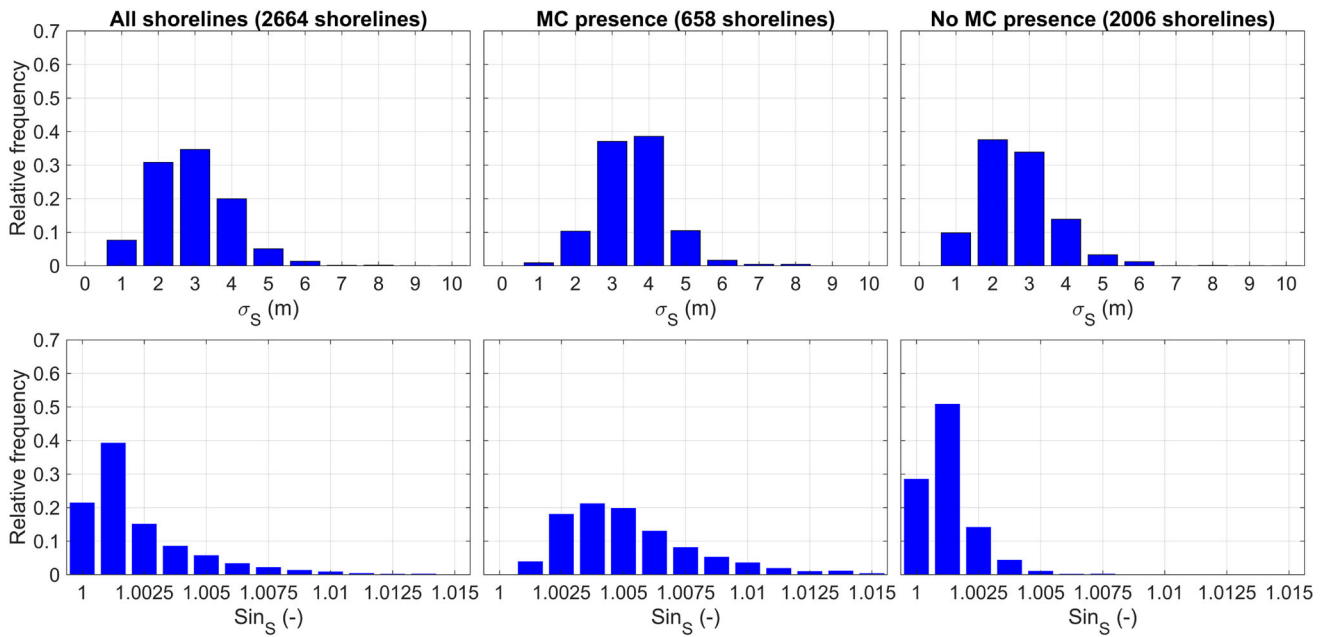
FIGURE 12 Histograms of the standard deviation of the shoreline σ_S (top) and the sinuosity of the shoreline Sin_S (bottom) for all shorelines (left), all shorelines with visually detected megacusps (middle) and without visually detected megacusps (right)

formation moments were not easy to detect as they often took more than 1 day, and the subtlety of the shoreline undulations made detection even more challenging. Conversely, detecting megacusp disappearance moments was generally easy when this was a result of wave activity as this usually occurred within 1 day. However, diffusion of megacusps during prolonged periods with low-energetic waves was more challenging because this generally occurred over several days. The small amplitudes of the megacusps could also partly explain why the sign of the cross-correlation did not always correctly discriminate between in phase and out of phase coupling (Section 3.3).

5.2 | Megacusp characteristics and dynamics

At Castelldefels, no clear relation was observed between megacusp formation, presence and disappearance and wave conditions. Low-energetic waves with a large variety in wave angles prevailed during megacusp presence, formation and absence (Figure 4b,c,d), whilst megacusp disappearance occurred both during higher and lower energetic waves with a similar variation in wave direction (Figure 4f). Similarly, no clear trend was observed in wave climate and directional spreading, which were similar during megacusp formation, presence and disappearance (Figures SI-4 and SI-5). In agreement with the Castelldefels observations, Segura et al. (2018) observed megacusp formation during lower energetic conditions and megacusp disappearance during both storms and extended periods of low-energetic waves. Other studies (e.g., Birrien et al., 2013; Castelle et al., 2019) observed accretive megacusps (located at the shoreline and similar to the Castelldefels megacusps) to generally disappear during storms. However, there are also observations at higher energetic coasts of megacusps persisting during storm conditions (Aagaard et al., 2005; Quartel, 2009) and Castelle et al. (2019) even observed the formation of large erosive megacusps (located at the dune foot and causing local dune erosion) during storms.

Megacusps at the study site displayed a wide variety in wavelengths (between 100 and 700 m; Figure 6d), whilst the amplitudes were less variable (generally between 3 and 7 m; Figure 6e). Compared to most previous observations (Table 4), the Castelldefels megacusps displayed relatively small wavelengths. Megacusp wavelengths are strongly related to those of crescentic bars (as will be discussed in Section 5.3) and their small sizes are probably due to the mostly low-energetic waves at the study site. However, Table 4 also shows examples of small megacusp wavelengths in higher energetic environments (e.g., Short, 1979; Thornton et al., 2007; Van de Lageweg et al., 2013) and larger wavelengths in low-energetic environments (Balouin et al., 2013). These variations in crescentic bar and megacusp wavelengths could also be related to variations in the bar–shoreline distance (De Swart et al., 2021). Megacusp migration rates at Castelldefels could reach 15 m/day, but were generally small (often even zero; Figure 6f). Previous studies observed fairly similar migration rates (Table 4) and megacusps were often also reported to be stationary (e.g., Galal & Takewaka, 2008; Segura et al., 2018). Megacusp migration at Castelldefels was not clearly linked to the radiation stress S_{xy} (Figure 9), which is another indication that waves are not the main driver of megacusp dynamics. This result might be site-dependent since Galal and Takewaka (2008) found a strong relation between alongshore currents and megacusp migration at their study site.

5.3 | Megacusp–crescentic bar coupling

Megacusp development at Castelldefels was strongly linked to crescentic bar presence. Megacusps generally developed a few days after the formation of a crescentic bar (first row of Table 2) and crescentic bars were present during most megacusp events (Table 1). This important role of sandbar geometry on shoreline dynamics and the resulting morphological coupling between megacusps and crescentic bars were observed by several previous studies (Table 4). Megacusps were

TABLE 4 Overview of previous observations of megacusps coupled to crescentic bars

Site	Tide (m)	H_{m0} (m)	$L_{y,MC}$ (m)	$A_{y,MC}$ (m)	$C_{y,MC}$ (m/day)	Coupling pattern	Study period	Reference
Cape Hatteras, USA[1]	1.1	1.3	550	10	5 (0–7)	−−	3 years[d]	Dolan (1971)
Various, USA[1]	−	−	−	−	−	−−	Variable[d]	Sonu (1973)
Various, USA[2]	−	−	−	−	−	++	Variable[d]	Sonu (1973)
White Park Bay, N-Ireland[1]	1.8	1.4	−	−	−	−−	≈ 5 years[b,d]	Carter and Kitcher (1979)
Various, Australia[1]	≈ 1.6	≈ 1.8	≈ 200	−	−	−−	> 2 years[b,d]	Short (1979)
HaHoterim, Israel[1]	0.6	1.2	−	−	−	−−	8 months[d]	Goldsmith et al. (1982)
HaHoterim, Israel[2]	0.6	1.2	−	−	−	++	8 months[d]	Goldsmith et al. (1982)
Various, Israel[1]	0.6	1.1	−	−	−	−−	32 years[d]	Bowman and Goldsmith (1983)
Hald, Denmark[1]	0.4	0.7	120	−	−	−−	5.5 months[b]	Aagaard (1988)
Various, Egypt[1]	≈ 0.3	≈ 1.1	125	−	−	−−	unknown[b,d]	Nafaa and Frihy (1993)
Monterey Bay, USA[1]	1.6	≈ 2.0	200	−	− (0–3.4)	−−	> 2 years[b,d]	Thornton et al. (2007)
Hasaki, Japan[1]	1.4	1.35	550	−	− (0–18)	−−	2 years[a]	Galal and Takewaka (2008)
Noordwijk, Netherlands[1]	1.8	≈ 1.0	243	−	≈ 3.5 (0–36)	+−	15 months[a]	Quartel (2009)
Monterey Bay, USA[1]	1.6	≈ 2.0	≈ 300	−	− (−)	+−	1–3 years[a]	Orzech et al. (2011)
Sète, France[1]	0.3	0.7	400	−	− (−)	−−	8 months[a,b]	Balouin et al. (2013)
Anglet, France[1]	3.9	1.6	450	≈ 15	− (−)	−−	18 months[a]	Birrien et al. (2013)
Tairua, New Zealand[1]	2.0	1.1	≈ 300	−	− (−)	+−	7 years[a]	Van de Lageweg et al. (2013)
Truc Vert, France[1]	5.0	1.8	400	10	2 (−)	++	12.5 years[b,c]	Castelle et al. (2015, 2019)
Truc Vert, France[3]	5.0	1.8	800	10	− (−)	−−	12.5 years[b,c]	Castelle et al. (2015, 2019)
Anmok, South Korea[1]	0.3	1.1	−	15	− (−)	+−	3 years[c]	Athanasiou et al. (2018)
Zandmotor, Netherlands[1]	1.7	1.0	−	−	− (−)	−−	2.4 years[a,b]	Rutten et al. (2018)
Secret Harbour, Australia[1]	< 0.5	≈ 0.8	150	3	− (0–20)	−−	2 years[a,b]	Segura et al. (2018)
Sylt, Germany[1]	2.0	≈ 0.9	2240	−	− (−)	−−	40 years[b]	Gijsman et al. (2021)
Castelldefels, Spain[1]	0.2	0.6	230	4	1.1 (0–15)	+−	≈ 8 years[a]	This study

Note: Site and megacusp characteristics are shown, as well as the dominant coupling pattern (following the definitions of Figure 2). Mean values are shown except tides (spring tidal range), C_y (absolute mean value and range) and coupling pattern (++ for in phase coupling, −− for out of phase coupling and +− for a mix of in phase and out of phase coupling).
Coupling detail: [1]shoreline–inner bar; [2]shoreline–outer bar; [3]dunefoot–outer bar. Dataset: [a]video data; [b]bathymetric data; [c]satellite data; [d]aerial photos.

typically coupled to the inner bar geometry, although some studies observed that the outer bar also affected the shoreline geometry (Table 4). In phase, out of phase and downwave coupling (definitions in Figure 2) occurred frequently at Castelldefels for all ranges in wave angle (Figure 10), whereas upwave coupling was only common for wave angles close to shore-normal. Previous studies mostly only distinguished between in phase and out of phase coupling, where out of phase coupling between the inner crescentic bars and megacusps was observed most frequently (Table 4). Furthermore, out of phase coupling is also the dominant coupling pattern in the beach classification scheme of Wright and Short (1984). Conversely, coupling between outer crescentic bars and megacusps was mostly reported to be in phase (e.g., Sonu, 1973).

During periods with significant sandbar–shoreline coupling at Castelldefels, the phases were often highly variable (Figures 7i, SI-6 and SI-7). This was linked to differential alongshore displacements of the crescentic bar with respect to the megacusps (Figure 11), since megacusps generally migrated much more slowly than crescentic bars (Figure 6f). Previous studies also reported that changes in phase were mainly related to different migration rates of the bar and shoreline (e.g., Quartel, 2009) and migration rates of crescentic bars were larger compared to those of megacusps (e.g., Balouin et al., 2013). Birrien

et al. (2013) also observed that megacusps were not able to swiftly adapt to quick alongshore migration of a crescentic bar.

5.4 | Interpretation of coupling patterns

Not many studies investigated what physical processes caused the formation of different coupling patterns between megacusps and inner crescentic bars, although there are a few modelling studies that obtained enlightening results. Calvete et al. (2005) found megacusp-like bedforms in the inner surf zone that were out of phase with the crescentic bars, which they attributed to the presence of a double rip cell circulation pattern (consisting of rip cells and counter-rotating cells near the shoreline) that was most evident during low-energetic waves and disappeared for higher energetic waves. Coco et al. (2020) obtained both in phase and out of phase coupling between megacusps and the inner crescentic bar (last column in their Figure 6), where out of phase coupling was accompanied by a double circulation pattern and a single circulation cell was present during in phase coupling. Orzech et al. (2011) found a strong dependence on the tide in their model results, with in phase coupling emerging for larger waves and higher tides and out of phase coupling emerging for smaller tides and

both smaller and larger waves. Generally, the above studies suggested that out of phase coupling develops during lower waves (favouring a double cell circulation; Figure 13a), whilst in phase coupling develops during larger waves (favouring a single cell circulation; Figure 13b).

Consistent with Calvete et al. (2005) and Coco et al. (2020), out of phase (in phase) coupling at Castelldefels was observed for lower (higher) energetic waves (Table 3 and Figure SI-8) and similar trends were reported by other observational studies (Balouin et al., 2013; Van de Lageweg et al., 2013). However, Orzech et al. (2011) observed (contrary to their modelling results) that in phase coupling was mostly present during small waves and higher tides, whilst out of phase coupling occurred during larger waves and smaller tides. Furthermore,

Van de Lageweg et al. (2013) also observed that the type of coupling was related to the bar-shoreline distance. This is consistent with the discussion in the previous paragraph, as a double (single) cell circulation can intuitively develop more easily when the bar is located far from (close to) shore, leading to out of phase (in phase) coupling. However, this was not evident in our observations at Castelldefels (Table 3 and Figure SI-9) because the average distances were much smaller (30–40 m) and more constant.

The most interesting result from Figure 10 is the abundance of downwave and the absence of upwave coupling (particularly during oblique waves). Since previous studies on sandbar–shoreline coupling mostly only discriminated between in phase and out of phase
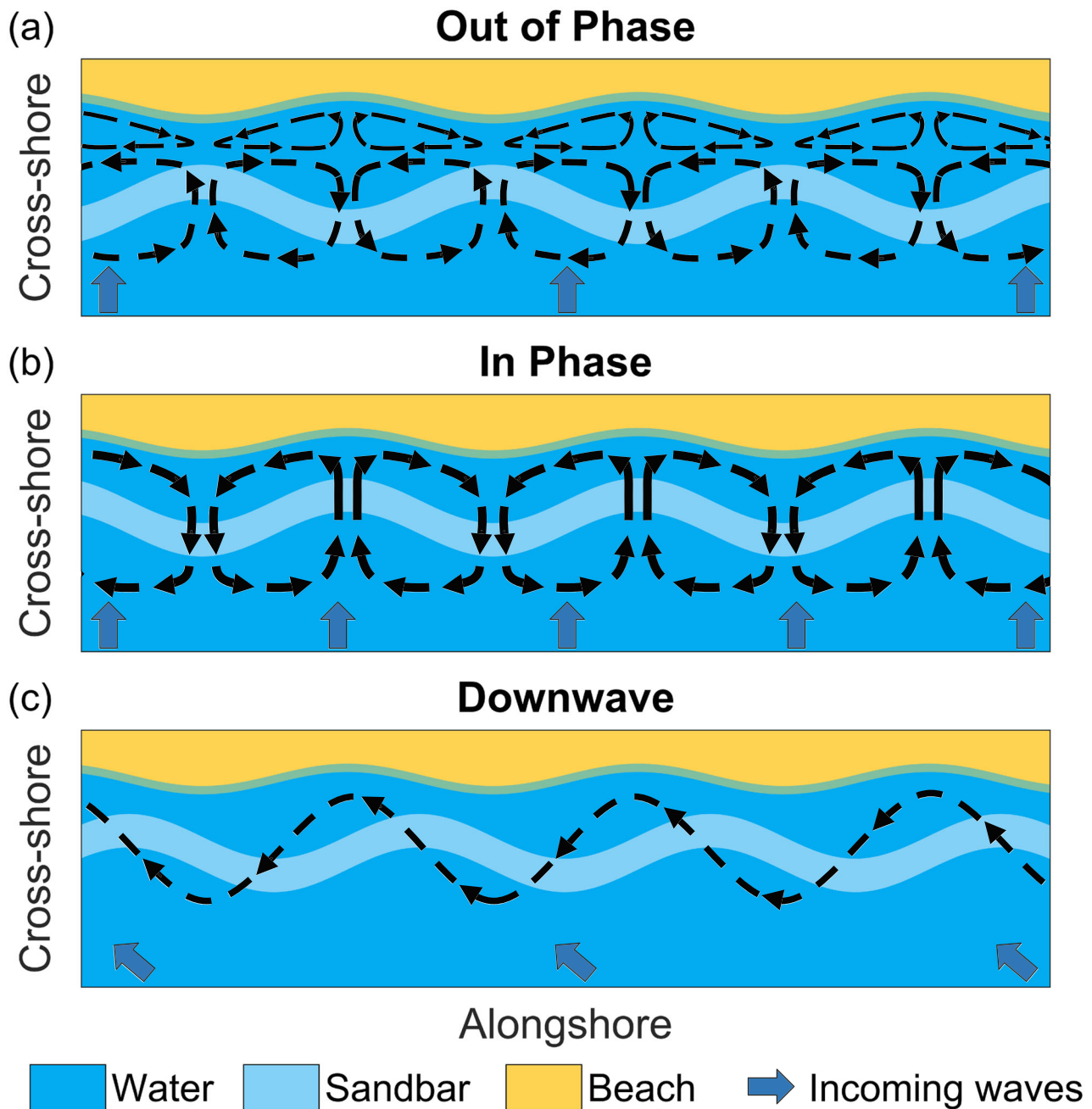

FIGURE 13 Idealised sketches of the current patterns during (a) out of phase, (b) in phase and (c) downwave coupling. For low-energetic and shore-normal waves, a double rip cell circulation is present (leading to out of phase coupling), whilst for higher energetic shore-normal waves a single rip cell develops (generating in phase coupling). For low-medium energetic waves with strong oblique angles of incidence, a meandering alongshore current develops, leading to downwave coupling. Panels (a) and (b) are inspired by the studies of Calvete *et al.* (2005) and Coco *et al.* (2020) and panel (c) is inspired by Sonu (1972)

coupling, it is generally unknown if a similar tendency also occurred at other beaches. However, similar downdrift coupling patterns have already been observed between outer and inner crescentic bars at the Gold Coast (horn of inner bar located downdrift of horn outer bar Price & Ruessink, 2013; Ruessink et al., 2007). These patterns were linked to strong oblique waves generating a meandering alongshore current over the inner crescentic bar that overwhelms the rip cell circulation patterns (MacMahan et al., 2010; Sonu, 1972), a hypothesis that was confirmed in a subsequent modelling study (Price et al., 2013). It is likely that the abundance of downwave coupling at Castelldefels is a result of a similar process. The often strong oblique wave angles at Castelldefels might drive a similar meandering alongshore current across the crescentic inner bar that is directed shoreward (seaward) at the inner bar horns (bays). At the location where this meandering current reaches a position closest to shore it may erode part of the shoreline and form a megacusp embayment downdrift of the crescentic bar horn, resulting in downwave coupling (Figure 13c; see also Figure 1 of Sonu, 1972).

6 | CONCLUSIONS

Megacusp dynamics and their coupling with crescentic bars were studied at the open, Mediterranean beach of Castelldefels using nearly 8 years of video images and directional wave conditions. During the study period, the alongshore-averaged shoreline retreated by about 8 m, and 67 megacusp events (including formation/straightening moments) were identified that lasted 706 days (24% of the time). Crescentic bars were present during 91% of the days with megacusps, whereas megacusps were only present during 50% of the days with crescentic bars. No clear relation between wave conditions and megacusps was observed, as low-energetic waves with a wide variety in direction prevailed during megacusp formation, presence and absence. Higher energetic waves prevailed during megacusp disappearance, although they also diffused during low-energetic wave conditions. Megacusps generally formed several days after the formation of a crescentic bar and they usually disappeared around the same time the crescentic bar straightened.

During the study period, megacusp and crescentic bar wavelengths were often similar (100–700 m), although considerable variations also occurred. The cross-shore amplitudes (3–8 m) and alongshore migration speeds (up to 15 m/day) of the megacusps were much smaller than those of the crescentic bars (5–20 m and up to 50 m/day, respectively). Megacusp migration was mostly triggered by crescentic bar migration and not clearly related to the radiation stress S_{xy}.

The coupling between megacusps and crescentic bars was significant at the 98% confidence level during 74% of the time with simultaneous presence of megacusps and crescentic bars (22% of the study period). Periods with significant coupling often showed large changes in phase which were linked to a displacement of the crescentic bar with respect to the megacusps. No dominant coupling pattern was observed, as in phase, out of phase and downwave (shoreline embayment downdrift of crescentic bar horn) coupling were regularly observed for all wave angles, whilst upwave (shoreline embayment updrift of crescentic bar horn) coupling was only common during waves with limited obliquity. Motivated by existing modelling studies,

it is hypothesised that out of phase (in phase) coupling develops in the presence of a double (single) rip cell circulation pattern. The prominence of downwave coupling is probably related to obliquely incident waves driving a meandering alongshore current over the inner crescentic bar, causing the formation of megacusp embayments downdrift of inner crescentic bar horns.

CONFLICT OF INTEREST

The authors declare that there are no conflicts of interest.

AUTHOR CONTRIBUTIONS

Conceptualization: R.d.S, F.R, D.C. Funding acquisition: F.R, D.C, G.S, J.G. Methodology: R.d.S, F.R, D.C. Investigation: R.d.S. Resources: R.d.S, F.R, G.S. Software: R.d.S, F.R, G.S. (g) Supervision: F.R, D.C. Writing—initial draft: R.d.S. Writing—reviewing and editing: R.d.S, F.R, D.C, G.S, J.G.

DATA AVAILABILITY STATEMENT

The research data from this study are available from the corresponding author upon reasonable request.

ORCID

Rinse L. de Swart https://orcid.org/0000-0001-6584-5184
Francesca Ribas https://orcid.org/0000-0003-4701-5982
Daniel Calvete https://orcid.org/0000-0002-5402-5137
Gonzalo Simarro https://orcid.org/0000-0002-6420-5975
Jorge Guillén https://orcid.org/0000-0001-7162-8135

REFERENCES

Aagaard T. (1988) Nearshore Bar Morphology on the Low-Energy Coast of Northern Zealand, Denmark. *Geografiska Annaler: Series A, Physical Geography*, 70(1-2), 59–67. https://doi.org/10.1080/04353676.1988.11880239

Aagaard T., Kroon A., Andersen S., Møller Sørensen R., Quartel S., Vinther N. (2005) Intertidal beach change during storm conditions; Egmond, The Netherlands. *Marine Geology*, 218(1–4), 65–80. https://doi.org/10.1016/j.margeo.2005.04.001

Athanasiou P., De Boer W., Yoo J., Ranasinghe R., Reniers A. (2018) Analysing decadal-scale crescentic bar dynamics using satellite imagery: A case study at Anmok beach, South Korea. *Marine Geology*, 405(August), 1–11. https://doi.org/10.1016/j.margeo.2018.07.013

Balouin Y., Tesson J., Gervais M. (2013) Cuspate shoreline relationship with nearshore bar dynamics during storm events - field observations at Sete beach, France. *Journal of Coastal Research*, 65(65), 440–445. https://doi.org/10.2112/si65-075.1

Birrien F., Castelle B., Dailloux D., Marieu V., Rihouey D., Price T. (2013) Video observation of megacusp evolution along a high-energy engineered sandy beach: Anglet, SW France. *Journal of Coastal Research*, 165(January), 1727–1732. https://doi.org/10.2112/si65-292.1

Bowman D., Goldsmith V. (1983) Bar morphology of dissipative beaches: An empirical model. *Marine Geology*, 51(1-2), 15–33. https://doi.org/10.1016/0025-3227(83)90086-5

Calvete D., Dodd N., Falqués A., van Leeuwen S.M. (2005) Morphological development of rip channel systems: Normal and near-normal wave incidence. *Journal of Geophysical Research C: Oceans*, 110(10), 1–18. https://doi.org/10.1029/2004JC002803

Carter R.W.G., Kitcher K.J. (1979) The Geomorphology of Offshore Sand Bars on the North Coast of Ireland. *Proceedings of the Royal Irish Academy. Section B: Biological, Geological, and Chemical Science*, 79, 43–61.

Castelle B., Marieu V., Bujan S. (2019) Alongshore-Variable Beach and Dune Changes on the Timescales from Days (Storms) to Decades Along the Rip-dominated Beaches of the Gironde Coast, SW France. *Journal of Coastal Research*, 88(sp1), 157. https://doi.org/10.2112/SI88-012.1

Castelle B., Marieu V., Bujan S., Splinter K.D., Robinet A., Sénéchal N., Ferreira S. (2015) Impact of the winter 2013-2014 series of severe Western Europe storms on a double-barred sandy coast: Beach and dune erosion and megacusp embayments. *Geomorphology*, 238, 135–148. https://doi.org/10.1016/j.geomorph.2015.03.006

Castelle B., Ruessink B.G. (2011) Modeling formation and subsequent nonlinear evolution of rip channels: Time-varying versus time-invariant wave forcing. *Journal of Geophysical Research*, 116(F4), F04008. https://doi.org/10.1029/2011JF001997

Castelle B., Ruessink B.G., Bonneton P., Marieu V., Bruneau N., Price T.D. (2010) Coupling mechanisms in double sandbar systems. Part 1: Patterns and physical explanation. *Earth Surface Processes and Landforms*, 35(4), 476–486. https://doi.org/10.1002/esp.1929

Coco G., Bryan K.R., Green M.O., Ruessink B.G., Turner I.L., Van Enckevort I.M.J. (2005) Video Observations of Shoreline and Sandbar Coupled Dynamics, Proceedings of Coasts and Ports.

Coco G., Calvete D., Ribas F., De Swart H.E., Falqués A. (2020) Emerging crescentic patterns in modelled double sandbar systems under normally incident waves. *Earth Surface Dynamics*, 8(2), 323–334. https://doi.org/10.5194/esurf-8-323-2020

Contardo S., Symonds G. (2015) Sandbar straightening under wind-sea and swell forcing. *Marine Geology*, 368, 25–41. https://doi.org/10.1016/j.margeo.2015.06.010

Crameri F. (2019) Scientific Colour Maps. https://doi.org/10.5281/zenodo.3596401

De Swart R.L., Ribas F., Calvete D., Kroon A., Orfila A. (2020) Optimal estimations of directional wave conditions for nearshore field studies. *Continental Shelf Research*, 196, 104071. https://doi.org/10.1016/j.csr.2020.104071

De Swart R.L., Ribas F., Simarro G., Guillén J., Calvete D. (2021) The role of bathymetry and directional wave conditions on observed crescentic bar dynamics. *Earth Surface Processes and Landforms*, 46(15), 3252–3270. https://doi.org/10.1002/esp.5233

Dolan R. (1971) Coastal landforms: Crescentic and rhythmic. *Bulletin of the Geological Society of America*, 82(1), 177–180. https://doi.org/10.1130/0016-7606(1971)82[177:CLCAR]2.0.CO;2

Galal E.M., Takewaka S. (2008) Longshore Migration of Shoreline Mega-Cusps Observed with X-Band Radar. *Coastal Engineering Journal*, 50(3), 247–276. https://doi.org/10.1142/S0578563408001818

Garnier R., Calvete D., Falqués A., Dodd N. (2008) Modelling the formation and the long-term behavior of rip channel systems from the deformation of a longshore bar. *Journal of Geophysical Research: Oceans*, 113(7), 1–18. https://doi.org/10.1029/2007JC004632

Garrett C., Toulany B. (1981) Variability of the flow through the Strait of Belle Isle. *Journal of Marine Research*, 39, 163–189.

Gijsman R., Ruessink B.G., Visscher J., Schlurmann T. (2021) Observations on decadal sandbar behaviour along a large-scale curved shoreline. *Earth Surface Processes and Landforms*, 46(2), 490–503. https://doi.org/10.1002/esp.5041

Goldsmith V., Bowman D., Kiley K. (1982) Sequential Stage Development of Crescentic Bars: Hahoterim Beach, Southeastern Mediterranean. *SEPM Journal of Sedimentary Research*, 52(1), 233–249. https://doi.org/10.1306/212F7F22-2B24-11D7-8648000102C1865D

Holthuijsen L.H. (2007) *Waves in Oceanic and Coastal Waters*. Cambridge University Press: Cambridge. https://doi.org/10.1017/CBO9780511618536

Lippmann T.C., Holman R.A. (1989) Quantification of sand bar morphology: a video technique based on wave dissipation. *Journal of Geophysical Research*, 94(C1), 995–1011. https://doi.org/10.1029/JC094iC01p00995

MacMahan J., Brown J., Brown J., Thornton E., Reniers A., Stanton T., et al. (2010) Mean Lagrangian flow behavior on an open coast rip-channeled beach: A new perspective. *Marine Geology*, 268(1–4), 1–15. https://doi.org/10.1016/j.margeo.2009.09.011

Nafaa M.G., Frihy O.E. (1993) Beach and nearshore features along the dissipative coastline of the Nile Delta, Egypt. *Journal of Coastal Research*, 9(2), 423–433.

Nieto M.A., Garau B., Balle S., Simarro G., Zarruk G.A., Ortiz A., et al. (2010) An open source, low cost video-based coastal monitoring system. *Earth Surface Processes and Landforms*, 35(14), 1712–1719. https://doi.org/10.1002/esp.2025

Ojeda E., Guillén J., Ribas F. (2011) Dynamics of single-barred embayed beaches. *Marine Geology*, 280(1–4), 76–90. https://doi.org/10.1016/j.margeo.2010.12.002

Orzech M.D., Reniers A.J.H.M., Thornton E.B., MacMahan J.H. (2011) Megacusps on rip channel bathymetry: Observations and modeling. *Coastal Engineering*, 58(9), 890–907. https://doi.org/10.1016/j.coastaleng.2011.05.001

Price T.D., Castelle B., Ranasinghe R., Ruessink B.G. (2013) Coupled sandbar patterns and obliquely incident waves. *Journal of Geophysical Research: Earth Surface*, 118(3), 1677–1692. https://doi.org/10.1002/jgrf.20103

Price T.D., Ruessink B.G. (2011) State dynamics of a double sandbar system. *Continental Shelf Research*, 31(6), 659–674. https://doi.org/10.1016/j.csr.2010.12.018

Price T.D., Ruessink B.G. (2013) Observations and conceptual modelling of morphological coupling in a double sandbar system. *Earth Surface Processes and Landforms*, 38(5), 477–489. https://doi.org/10.1002/esp.3293

Puertos del Estado. (1994) Maritime Works Recommendations. ROM 0.3-91 Waves Annex 1: Wave Climate on the Spanish coast, Ministerio de Obras Publicas y Transporte, Centro de Publicaciones de Secretaría General Técnica.

Quartel S. (2009) Temporal and spatial behaviour of rip channels in a multiple-barred coastal system. *Earth Surface Processes and Landforms*, 34(2), 163–176. https://doi.org/10.1002/esp.1685

Ribas F., Simarro G., Arriaga J., Luque P. (2020) Automatic Shoreline Detection from Video Images by Combining Information from Different Methods. *Remote Sensing*, 12(22), 3717. https://doi.org/10.3390/rs12223717

Ruessink B.G., Coco G., Ranasinghe R., Turner I.L. (2007) Coupled and non-coupled behavior of three-dimensional morphological patterns in a double sandbar system. *Journal of Geophysical Research: Oceans*, 112(7), 1–11. https://doi.org/10.1029/2006JC003799

Rutten J., Ruessink B.G., Price T.D. (2018) Observations on sandbar behaviour along a man-made curved coast. *Earth Surface Processes and Landforms*, 43(1), 134–149. https://doi.org/10.1002/esp.4158

Segura L.E., Hansen J.E., Lowe R.J., Symonds G., Contardo S. (2018) Shoreline variability at a low-energy beach: Contributions of storms, megacusps and sea-breeze cycles. *Marine Geology*, 400(March), 94–106. https://doi.org/10.1016/j.margeo.2018.03.008

Short A.D. (1979) Three Dimensional Beach-Stage Model. *The Journal of Geology*, 87(5), 553–571. https://doi.org/10.1086/628445

Simarro G., Bryan K.R., Guedes R.M.C., Sancho A., Guillen J., Coco G. (2015) On the use of variance images for runup and shoreline detection. *Coastal Engineering*, 99, 136–147. https://doi.org/10.1016/j.coastaleng.2015.03.002

Simarro G., Ribas F., Álvarez A., Guillén J., Chic O., Orfila A. (2017) ULISES: An Open Source Code for Extrinsic Calibrations and Planview Generations in Coastal Video Monitoring Systems. *Journal of Coastal Research*, 335, 1217–1227. https://doi.org/10.2112/JCOASTRES-D-16-00022.1

Sonu C.J. (1972) Field observation of nearshore circulation and meandering currents. *Journal of Geophysical Research*, 77(18), 3232–3247. https://doi.org/10.1029/JC077i018p03232

Sonu C.J. (1973) Three-Dimensional Beach Changes. *The Journal of Geology*, 81(1), 42–64. https://doi.org/10.1086/627806

Thornton E.B., MacMahan J., Sallenger A.H. (2007) Rip currents, megacusps, and eroding dunes. *Marine Geology*, 240(1–4), 151–167. https://doi.org/10.1016/j.margeo.2007.02.018

Van Enckevort I.M.J., Ruessink B.G., Coco G., Suzuki K., Turner I.L., Plant N.G. et al. (2004) Observations of nearshore crescentic sandbars. *Journal of Geophysical Research*, 109(C6), C06028. https://doi.org/10.1029/2003JC002214

Van de Lageweg W.I., Bryan K.R., Coco G., Ruessink B.G. (2013) Observations of shoreline-sandbar coupling on an embayed beach. *Marine Geology*, 344, 101–114. https://doi.org/10.1016/j.margeo.2013.07.018

Wright L.D., Short A.D. (1984) Morphodynamic variability of surf zones and beaches: A synthesis. *Marine Geology*, 56(1–4), 93–118. https://doi.org/10.1016/0025-3227(84)90008-2

SUPPORTING INFORMATION

Additional supporting information can be found online in the Supporting Information section at the end of this article.

How to cite this article: de Swart, R.L., Ribas, F., Calvete, D., Simarro, G. & Guillén, J. (2022) Observations of megacusp dynamics and their coupling with crescentic bars at an open, fetch-limited beach. *Earth Surface Processes and Landforms*, 1–19. Available from: https://doi.org/10.1002/esp.5451